

**A 13 million-year record of Li isotope compositions in island carbonates: constraints on  
bulk inorganic carbonate as a global seawater Li isotope archive**

Guang-Yi Wei<sup>1</sup>, Feifei Zhang<sup>1\*</sup>, Yi-Sheng Yin<sup>1</sup>, Yi-Bo Lin<sup>1</sup>, Philip A. E. Pogge von  
Strandmann<sup>2</sup>, Mengchun Cao<sup>1</sup>, Na Li<sup>1,3</sup>, Guolin Xiong<sup>1</sup>, Xinran Chen<sup>1</sup>, Caiwei Fan<sup>4</sup>,  
Changgui Xu<sup>4</sup>, Fei Tan<sup>5</sup>, Xiyang Zhang<sup>5</sup>, Hongqiang Yang<sup>5</sup>, Hong-Fei Ling<sup>1</sup>, Shu-Zhong  
Shen<sup>1</sup>

<sup>1</sup>  
*State Key Laboratory for Mineral Deposits Research, School of Earth Sciences and  
Engineering and Frontiers Science Center for Critical Earth Material Cycling, Nanjing  
University, 163 Xianlin Avenue, Nanjing 210023, China*

<sup>2</sup>  
*Institute of Geosciences, Johannes Gutenberg University, 55122 Mainz, Germany*

<sup>3</sup>  
*School of Geography and Ocean Science, Nanjing University, 163 Xianlin Avenue, Nanjing  
210023, China*

<sup>4</sup>  
*Zhanjiang Branch of China National Offshore Oil Corporation Ltd., Zhanjiang, Guangdong  
524057, China*

<sup>5</sup>  
*Key Laboratory of Ocean and Marginal Sea Geology, South China Sea Institute of Oceanology  
of Sciences, Innovation Academy of South China Sea Ecology and Environmental Engineering,  
Chinese Academy of Sciences, Guangzhou 510301, China*

\* Corresponding author: [fzhang@nju.edu.cn](mailto:fzhang@nju.edu.cn) (Feifei Zhang)

**Abstract**

Lithium isotope ( $\delta^7\text{Li}$ ) variations in marine carbonate sediments and rocks have been  
widely used to reconstruct global seawater Li isotope compositions and then trace  
paleo-weathering processes. However, there are still debates on whether ancient carbonates  
can faithfully document original seawater  $\delta^7\text{Li}$  signals, as  $\delta^7\text{Li}$  values of shallow-water  
carbonates are tightly related to carbonate mineralogy and diagenetic alteration. In this study,  
we present high-resolution  $\delta^7\text{Li}$ , trace element and carbonate mineralogy data of shallow-

28 water carbonate deposits from two shallow drillcores (Jiuzhang A and B) and a deep drillcore  
29 (XK-1) in the South China Sea. We compare these new  $\delta^7\text{Li}$  data to the ca. 13 Myr history of  
30 seawater  $\delta^7\text{Li}$  evolution from the middle Miocene to Pleistocene, in order to better constrain  
31 the effects of carbonate mineralogy and early diagenesis on  $\delta^7\text{Li}$  values of bulk inorganic  
32 carbonates. We observe that the  $\delta^7\text{Li}$  values of primary carbonate deposits in Jiuzhang A, B  
33 and the uppermost XK-1 drillcores ( $24.6\text{‰} \pm 1.6\text{‰}$ ,  $n = 37$ ,  $1\sigma$ ) are significantly lower than  
34 modern seawater  $\delta^7\text{Li}$  values ( $\Delta^7\text{Li}_{\text{primary-seawater}} = \sim -6.0\text{‰}$ ). In contrast, marine diagenetic  
35 carbonates in the XK-1 drillcore exhibit  $\delta^7\text{Li}$  values of  $28.7\text{‰} \pm 0.7\text{‰}$  ( $n = 54$ ,  $1\sigma$ ),  
36 approaching coeval seawater values ( $\Delta^7\text{Li}_{\text{marine diagenetic-seawater}} = \sim -2.0\text{‰}$ ) and much higher than  
37 those of primary carbonate deposits. Meteoric diagenetic carbonates in the XK-1 drillcore  
38 show  $\delta^7\text{Li}$  values of  $22.4\text{‰} \pm 1.6\text{‰}$  ( $n = 46$ ,  $1\sigma$ ), close to that of primary carbonate deposits  
39 in Jiuzhang A, B and the uppermost XK-1 drillcores, but significantly lower than coeval  
40 seawater  $\delta^7\text{Li}$  values ( $\Delta^7\text{Li}_{\text{meteoric diagenetic-seawater}} = -5.0\text{‰}$  to  $-9\text{‰}$ ). Such  $\delta^7\text{Li}$  variations in  
41 shallow-water carbonates are attributed to variations in carbonate mineralogy (i.e., aragonite,  
42 high-Mg calcite and low-Mg calcite) and diagenetic regimes (fluid- or sediment-buffered  
43 conditions of marine and meteoric diagenesis). By comparing  $\delta^7\text{Li}$  data from the South China  
44 Sea to those from the Bahamas, we suggest strongly fluid-buffered conditions for Li isotopes  
45 during marine diagenesis, resulting in  $\delta^7\text{Li}$  values of marine limestones and dolostones  
46 approaching ambient seawater  $\delta^7\text{Li}$  signals. In contrast, meteoric diagenetic carbonates, likely  
47 marked by sediment-buffered conditions, may inherit the original  $\delta^7\text{Li}$  signals of primary  
48 carbonate deposits. Hence, full considerations of the carbonate mineralogy and diagenesis  
49 facilitate a better use of bulk carbonate-archived  $\delta^7\text{Li}$  to reconstruct paleo-weathering

evolution in deep time lacking the skeletal fossil records.

**Keywords:** lithium isotope; shallow-water carbonates; South China Sea; diagenesis;

Neogene; paleo-weathering proxy

## 1. Introduction

Following substantial research over the last 30 years, lithium (Li) and its isotopic compositions ( $\delta^7\text{Li}$ ) have emerged as promising proxies for continental silicate weathering, based on modern frameworks that Li isotope fractionations on the Earth's surface are closely linked to the silicate weathering process (see reviews in Tomascak et al., 2016; Penniston-Dorland et al., 2017; Pogge von Strandmann et al., 2020, 2021a). With main Li inputs from rivers and high-temperature hydrothermal fluids at mid-ocean ridges, modern seawater has a long residence time of Li ( $\sim 1$  Myr) and homogeneous  $\delta^7\text{Li}$  values ( $\sim 31\text{‰}$ ) (Lécuyer et al., 2016; Millot et al., 2004; Hathorne and James, 2006; Misra and Froelich, 2012). Regulated by riverine Li flux and  $\delta^7\text{Li}$  value that relate to continental silicate weathering and hydrological conditions (Huh et al., 1998; Pogge von Strandmann et al., 2006, 2017b; Vigier et al., 2009; Millot et al., 2010; Dellinger et al., 2015; Murphy et al., 2019; Zhang et al., 2022), the evolution of  $\delta^7\text{Li}$  and Li concentrations of paleo-seawater provides valuable insights into global average silicate weathering regimes through geological time. Therefore, how to precisely and effectively trace  $\delta^7\text{Li}$  variations in paleo-seawater is critical to applying Li isotopes as a paleo-weathering proxy. Marine carbonates (biogenic carbonates or inorganic carbonate deposits) have been considered as an archive for seawater  $\delta^7\text{Li}$  signals and have been widely used to reconstruct paleo-seawater Li isotope compositions (Hathorne and James, 2006; Misra and Froelich, 2012; Pogge von Strandmann et al., 2013, 2017a,

2021b; Ullmann et al., 2013; Lechler et al., 2015; Washington et al., 2020; Kalderon-Asael et al., 2021).

Prior laboratory and natural investigations of Li isotope behavior during carbonate mineral precipitation (both biogenic and inorganic carbonate minerals) show highly variable  $\delta^7\text{Li}$  values, dependent on carbonate mineralogy (Marriott et al., 2004a, b; Dellinger et al., 2018; Pogge von Strandmann et al., 2019), species-specific effects (Hathorne and James, 2006; Rollion-Bard et al., 2009; Bastian et al., 2018; Dellinger et al., 2018; Washington et al., 2020), along with solution chemistry, pH and growth rate (Gabitov et al., 2011; Vigier et al., 2015; Roberts et al., 2018; Day et al., 2021; Seyedali et al., 2021; Fuger et al., 2022). Despite disputes over the effects of foraminiferal species (Hathorne and James, 2006; Misra and Froelich, 2012) and solution chemistry (e.g., pH) (Rollion-Bard et al., 2009; Vigier et al., 2015; Roberts et al., 2018), carbonate mineralogy may have played a fundamental control on the  $\delta^7\text{Li}$  values of marine biogenic carbonates (Dellinger et al., 2018) and bulk carbonate deposits (Pogge von Strandmann et al., 2019; Dellinger et al., 2020). With high consistency in the results of natural and synthetic carbonates, primary aragonite generally has significantly larger Li isotope fractionations relative to parent solutions ( $\Delta^7\text{Li}_{\text{aragonite-solution}} = -7\text{‰} \sim -12\text{‰}$ ), whereas primary low-Mg calcite tends to show smaller Li isotope fractionations than aragonite ( $\Delta^7\text{Li}_{\text{calcite-solution}} = -2\text{‰} \sim -7\text{‰}$ ) and high-Mg calcite may have fractionations between aragonite and low-Mg calcite (Marriott et al., 2004a,b; Rollion-Bard et al., 2009; Gabitov et al., 2011; Bastian et al., 2018; Pogge von Strandmann et al., 2019; Dellinger et al., 2018, 2020). In this light, it is important to fully evaluate changes in carbonate mineralogy through geological time (e.g., Holland, 2005) when reconstructing long-term seawater  $\delta^7\text{Li}$



using the carbonate archive. Further, research on the  $\delta^7\text{Li}$  of bulk inorganic carbonates, particularly shallow-water carbonates, requires more consideration of diagenetic processes (early marine diagenesis or meteoric diagenesis) that have been verified to notably alter many other isotope systems (e.g.,  $\delta^{13}\text{C}$ ,  $\delta^{18}\text{O}$ ,  $\delta^{44}\text{Ca}$ ,  $\delta^{11}\text{B}$ ,  $\delta^{238}\text{U}$ ). For example, neomorphism or dolomitization of primary aragonite during the marine diagenesis can highly increase  $\delta^{44}\text{Ca}$  values of shallow-water carbonates (Higgins et al., 2018). The meteoric diagenetic alteration (i.e., an early diagenetic process occurring in freshwater environment) would notably alter the  $\delta^{13}\text{C}$ ,  $\delta^{18}\text{O}$ ,  $\delta^{11}\text{B}$  and  $\delta^{238}\text{U}$  signals of primary carbonates (Swart, 2015; Stewart et al., 2015; Chen et al., 2018; Tissot et al., 2018). Yet so far, very few studies have been conducted to constrain the Li isotope behavior during different diagenetic processes of modern bulk carbonates, and Li isotope offsets between carbonate and ambient seawater or pore fluid (Andrews et al., 2020; Dellinger et al., 2020; Murphy et al., 2022). Due to the relative scarcity of  $\delta^7\text{Li}$  data of shallow-water carbonates under different diagenetic regimes and mineralogy, it is still disputed how abiotic carbonate  $\delta^7\text{Li}$  values change during the different diagenetic regimes, including fluid- or sediment buffered marine diagenesis (i.e., diagenesis is dominated by the chemistry of the fluid or the chemistry of the sediment), meteoric diagenesis (i.e., freshwater as the diagenetic fluid), (syn)dolomitization, and whether the diagenetic alteration of primary carbonate  $\delta^7\text{Li}$  signals is globally representative. Additionally, given the relatively variable  $\delta^7\text{Li}$  values of different carbonate minerals and species, there are doubts about which type of carbonate deposits can faithfully record the Li isotope compositions of coeval seawater.

In this study, we report high-resolution Li content and  $\delta^7\text{Li}$  data of island carbonates

from one deep drillcore (XK-1), two shallow drillcores (A and B), and shallow-water corals in the South China Sea (Fig. 1). We aim to reconstruct the past 13 million years of carbonate diagenetic history (from the middle Miocene to the present) for Li isotopes to better evaluate the use of shallow-water carbonates as an archive for seawater Li isotope compositions. With independent evidence for different early diagenetic zones in these drillcores, we aim to conduct more systematic investigations on  $\delta^7\text{Li}$  variations controlled by different early diagenetic processes and carbonate mineralogy of shallow-water carbonates. By comparing the data from South China Sea carbonates to those from other Quaternary carbonates (e.g., the Bahamian carbonates), we further evaluate the effects of different diagenetic regimes (i.e., meteoric diagenesis, marine diagenesis under fluid- or sediment-buffered conditions, marine dolomitization) on  $\delta^7\text{Li}$  values of shallow-water carbonates, and then provide more insights for using shallow-water carbonate as a reliable archive for global seawater  $\delta^7\text{Li}$  signals in deep time.

## 2. Samples

Two sets of shallow-water corals (8 samples) were collected from the town of Paipu, Hainan Island (19°39'27.56"N, 109°05'44.43"E) and the Jiuzhang Reefs, Nansha Islands (9°57'55"N, 114°36'14"E) in the South China Sea (Fig. 1). The analyzed coral skeletons included various species: *Porites lutea*, *Acropora parilis*, *Fungia fungites*, *Favites abdita* from the Hainan Island and *Porites lobata*, *Goniopora tenuidens*, *Goniastrea minuta*, *Galaxea fascicularis* from the Nansha Islands.

A total of 346 bulk carbonate samples, dominated by inorganic carbonate deposits (> 90%) along with small amounts of bioclastic, were collected from one deep drillcore (XK-1)

on Shidao (Rocky) Island of Xisha (16°50'N, 112°20'E), northwestern South China Sea, and two shallow drillcores (A and B) on the Jiuzhang Giant Atoll of Nansha Island (9°42'–10°00'N, 114°15'–114°40'E), southern South China Sea (Fig. 1). The selected carbonate succession from the XK-1 drillcore is ~700 m thick and mainly consists of algal-reef and bioclastic limestone and dolostone, representing deposition on an elevated submarine plateau with a modern relief of +1.5 m on its top (Shao et al., 2017a,b). The porosity of the XK-1 drillcore is ~0.4, similar to that of Bahamian sediments (Melim et al., 2002). A four-stage post-depositional model has been reconstructed for the XK-1 drillcore, including 1) sea-level fall and meteoric diagenesis in the late stage of the middle Miocene (600–650 mbsf); 2) sea-level rise and marine diagenesis from the upper Miocene to the Pliocene (200–600 mbsf); 3) oscillating and low sea-level and meteoric diagenesis during the Pleistocene (25–200 mbsf); and 4) sea-level rise from the uppermost Pleistocene and primary carbonate precipitates (0–25 mbsf) (Shao et al., 2017a). The shallow drillcore A and B are ~4.75 m and ~2.55 m thick, respectively. Core A (9°55'56.75"N, 114°31'19.55"E) lies in the interior barrier lagoon of one square kilometer at a water depth of ~10 meters, and Core B (9°57'38.54"N, 114°34'12.74"E) is located within the reef flat of Holiday Reef with a water depth of several meters. The carbonate sediments in cores A and B mainly comprise unlithified carbonate sands/muds (< 1mm grain size) and visible coarse-grained bioclastics (1–2 mm) without seagrass and hard substrates (e.g., chunks of coral heads), representing recent carbonate deposits (< 1000 years).

### 3. Methods

#### 3.1 X-Ray Diffraction (XRD) analysis

Carbonate mineralogy of the studied bulk carbonates was determined using a Bruker D8

Advance X-ray diffractometer at the State Key Laboratory for Mineral Deposits Research, Nanjing University. The diffraction spectral pattern was measured at a  $2\theta$  step scan of  $0.01^\circ$  between  $20^\circ$  and  $60^\circ$ . The limit of detection for minerals is 0.1 cps for peak intensity. Quantitative determination of percentage compositions for different carbonate minerals was performed using the XRD data with whole-pattern fitting and Rietveld refinement with DIFFRAC.EVA V4.3.2 software. The error of carbonate mineralogical proportions is the 0.35 power of each percentage.

### 3.2 Carbon and oxygen isotope analysis

Approximately 5  $\mu\text{g}$  sample powder was reacted with orthophosphoric acid at  $75^\circ\text{C}$  for 12 h to fully liberate  $\text{CO}_2$  from the carbonate minerals following the principles first determined by McCrea (1950) and Craig (1953). Carbon and oxygen isotopes were measured with an online analysis system, Finnigan Gas-bench II + Delta Plux XP at the State Key Laboratory for Mineral Deposits Research, Nanjing University. Based on acid isotopic fractionation factors for different carbonate minerals (e.g., Kim et al., 2007 and references therein), the results of C–O isotopes are calculated using a two-point linear normalization approach and ultimately reported relative to VPDB. The external analytical precision for C and O isotopes is  $0.06\text{‰}$  and  $0.07\text{‰}$  ( $2\sigma$ ), respectively, based on replicate analyses of the Chinese GBW04416 ( $\delta^{13}\text{C} = 1.61\text{‰} \pm 0.06\text{‰}$ ;  $\delta^{18}\text{O} = -11.56\text{‰} \pm 0.07\text{‰}$ ) and GBW04417 ( $\delta^{13}\text{C} = -6.06\text{‰} \pm 0.06\text{‰}$ ;  $\delta^{18}\text{O} = -24.12\text{‰} \pm 0.07\text{‰}$ ) carbonate standards.

### 3.3 Lithium isotope analysis

A total of 145 bulk carbonate and coral skeleton samples were selected for Li isotope analysis, in which a sequential leaching method was used to extract the Li in the carbonate component of bulk samples. Approximately 400 mg bulk carbonate powders were first rinsed using 1 N ammonium acetate to eliminate exchangeable Li adsorbed onto bulk carbonate. The residual samples were rinsed and then digested using 1 N acetic acid for 4 hours to dissolve the carbonate component. Four batches of samples were dissolved following above procedure

together with one blank and two carbonate standards (GSR-6 limestone standard and GSR-12 dolostone standard) in each batch.

Trace and major elemental concentrations of the acetic acid leachates were measured on an Agilent 7900 Quadrupole ICP–MS with RSD <5%, based on repeated analyses of the rock standard BHVO-2 and OSIL Atlantic seawater at Nanjing University. The trace and major elemental contents of the studied samples are calculated using the data of acetic acid leachates and total weights of each sample, representing the pure carbonate component of bulk samples. The carbonate standard GSR-6 and GSR-12 have low Li concentrations in their pure carbonate components ( $[Li]_{GSR-6} = 0.4 \mu\text{g/g}$ ;  $[Li]_{GSR-12} = 1.6 \mu\text{g/g}$ ), similar to those of carbonate samples in this study. A calibrated single column method with AG50 W-X12 cation resin was used to purify Li in the carbonate component with 0.5 N and 0.2 N HCl based on the calculation of Li/(Ca+Mg) ratios for each sample (see Supplementary materials for details). The Li yield after the chromatographic step was > 99%, based on checking Li concentrations of the solution before and after the Li elution interval. The purified sample solution was measured on a Thermo Scientific Finnigan Neptune plus MC–ICP–MS at the MOE Key Laboratory of Surficial Geochemistry, Nanjing University. Using a Sample-Standard Bracketing (SSB) method, the Li isotopes of each sample were normalized to the L-SVEC Li isotope standard:

$$\delta^7\text{Li} = (^7\text{Li}/^6\text{Li}_{\text{sample}} / ^7\text{Li}/^6\text{Li}_{\text{L-SVEC}} - 1) \times 1000$$

The Li concentrations of the samples and standards were matched to ~20 ng/mL with uncertainties of  $\pm 10\%$  in 2 mL solution, to avoid the potential effect of concentration mismatches between the sample and standard solutions. The total procedural blank for each sample digestion, Li purification and analysis is < 0.1 ng, which is significantly lower than those of measured samples (~40 ng). An in-house Li solution (GAGS-Li,  $\delta^7\text{Li} = 15.3\text{‰} \pm 0.5\text{‰}$ ,  $2\sigma$ ,  $n = 60$  every 3 samples over 6 months analyses) and OSIL Atlantic seawater ( $\delta^7\text{Li} = 30.7\text{‰} \pm 0.4\text{‰}$ ,  $2\sigma$ ,  $n = 15$ ) was used to monitor the long-term reproducibility of Li isotope analyses on the machine. The overall reproducibility and accuracy of the total procedure (sample digestion, Li separation and isotope measurement) were checked by repeated analyses of carbonate standards GSR-6 ( $\delta^7\text{Li} = -1.75 \pm 0.5\text{‰}$ ,  $2\sigma$ ,  $n=4$ ) and GSR-12 ( $\delta^7\text{Li} = 13.5 \pm 0.6\text{‰}$ ,

2 $\sigma$ , n=4), with different aliquots processed through column chemistry (Lin et al., 2019; Zhu et al., 2019). The final external analytical precision in this study is considered better than  $\pm 0.6\%$  ( $2\sigma$ ), based on the repeated measurements of in-house Li solution, purified seawater and carbonate standards.

#### 4. Results

The results of scanning electron microcopy (SEM) and XRD analysis for the carbonate mineralogy are presented as the proportions of aragonite, high-Mg calcite, low-Mg calcite and dolomite in Figs. 2 and 3. The major/trace element and  $\delta^{13}\text{C}$ ,  $\delta^{18}\text{O}$ , and  $\delta^7\text{Li}$  data of the XK-1, Jiuzhang A and B drillcores and coral samples are shown in Figs. 3–6 (see Supplementary table for data compilations). Additional data (i.e., molar ratios of  $\text{Mg}/(\text{Ca}+\text{Mg})$ ,  $\text{Li}/(\text{Ca}+\text{Mg})$ ,  $\text{Sr}/(\text{Ca}+\text{Mg})$ ) are also examined to better constrain differences in carbonate components and diagenetic regimes of bulk samples, which are presented in detail in the supplementary table. The Jiuzhang A and B drillcores, dominated by aragonite and high-Mg calcite precipitates, show similar and relatively uniform  $\delta^{13}\text{C}$  values from 0.9‰ to 2.1‰,  $\delta^{18}\text{O}$  values from  $-3.9\%$  to  $-3.0\%$ ,  $\delta^7\text{Li}$  values from 22.3‰ to 25.0‰, Li contents from 0.3  $\mu\text{g/g}$  to 1.2  $\mu\text{g/g}$ , and Sr contents from 2844  $\mu\text{g/g}$  to 5478  $\mu\text{g/g}$ . The coral samples show  $\delta^7\text{Li}$  values from 16.1‰ to 19.4‰,  $\delta^{13}\text{C}$  values from  $-6.7\%$  to  $-1.3\%$ ,  $\delta^{18}\text{O}$  values from  $-5.7\%$  to  $-4.8\%$ , along with high Sr contents from 1727  $\mu\text{g/g}$  to 8397  $\mu\text{g/g}$  and low Li contents from 0.1  $\mu\text{g/g}$  to 0.4  $\mu\text{g/g}$ .

Throughout the XK-1 drillcore, the samples exhibit largely varying  $\delta^7\text{Li}$ ,  $\delta^{13}\text{C}$ ,  $\delta^{18}\text{O}$  values, and Li and Sr contents. The uppermost interval of the XK-1 drillcore ( $> -25$  m), consisting of aragonites, high-Mg calcites and low-Mg calcites, have relatively uniform  $\delta^7\text{Li}$  values from 23.1‰ to 26.3‰,  $\delta^{13}\text{C}$  values from  $-1.3\%$  to 1.7‰,  $\delta^{18}\text{O}$  values from  $-6.0\%$  to  $-0.9\%$  with

high Li (from 0.3  $\mu\text{g/g}$  to 1.4  $\mu\text{g/g}$ ) and Sr contents (from 1716  $\mu\text{g/g}$  to 4898  $\mu\text{g/g}$ ), which are overall close to those of Jiuzhang A and B cores. The interval from –25 m to –400 m in the XK-1 core mainly comprises low-Mg calcites and exhibits large negative excursions of  $\delta^7\text{Li}$  (from 30.1‰ to 20.2‰),  $\delta^{13}\text{C}$  (from 1.6‰ to –4.0‰),  $\delta^{18}\text{O}$  (from 2.1‰ to –8.7‰) and Li contents (from 1.2  $\mu\text{g/g}$  to 0.15  $\mu\text{g/g}$ ), along with decreased Sr contents (from 3307  $\mu\text{g/g}$  to 373  $\mu\text{g/g}$ ). The interval from –400 m to –575 m is dominated by dolomites with high values of  $\delta^7\text{Li}$  (from 26.5‰ to 29.4‰),  $\delta^{13}\text{C}$  (from 1.5‰ to 2.7‰),  $\delta^{18}\text{O}$  (from 1.9‰ to 3.5‰) and Li contents (from 1.1  $\mu\text{g/g}$  to 1.5  $\mu\text{g/g}$ ) but low Sr contents (from 172  $\mu\text{g/g}$  to 470  $\mu\text{g/g}$ ). The lowest interval from –580 m to –607 m, marked by low-Mg calcites with low Sr contents (from 315  $\mu\text{g/g}$  to 523  $\mu\text{g/g}$ ), has appreciable negative excursions of  $\delta^7\text{Li}$  (from 24.7‰ to 21.8‰),  $\delta^{13}\text{C}$  (from 1.8‰ to –2.7‰),  $\delta^{18}\text{O}$  (from –0.7‰ to –5.7‰) and Li contents (from 1.1  $\mu\text{g/g}$  to 0.4  $\mu\text{g/g}$ ).

## 5. Discussion

The Al/(Ca+Mg) ratios of the studied carbonates are first used to evaluate the effects of detrital contamination on  $\delta^7\text{Li}$  values, as carbonates commonly have low Li contents and are susceptible to Li contamination from clays during sample digestion (Pogge von Strandmann et al., 2013; Kalderon-Asael et al., 2021). The studied carbonates have relatively low Al/(Ca+Mg) ratios (~0.34 mmol/mol on average), similar to those in the Bahamas (Dellinger et al., 2020), suggesting negligible effects of detrital contamination on carbonate  $\delta^7\text{Li}$  values (0.8 mmol/mol was previously chosen as a threshold value, Pogge von Strandmann, 2013). In this discussion, we mainly explore the influences of mineralogy, early diagenesis (dolomitization) and other potential factors on Li isotope compositions of bulk shallow-water

263 carbonates.

## 264 5.1 Potential factors controlling $\delta^7\text{Li}$ values of shallow-water carbonates in the South China 265 Sea

266 Skeletons of the studied shallow-water corals from the South China Sea are dominated  
267 by aragonite precipitates, marked by significantly high Sr and low Li contents (e.g., Rollion-  
268 Bard et al., 2009; Gabitov et al., 2011; Bastian et al., 2018; Dellinger et al., 2018). The  
269 unconsolidated carbonate sediments in the Jiuzhang A and B cores mainly comprise aragonite  
270 and high-Mg calcite, along with very small amounts of low-Mg calcite (Fig. 3). The carbonate  
271 mineralogy varies throughout the XK-1 drillcore, including mixing of aragonite, high-Mg  
272 calcite and low-Mg calcite (0–25 m), low-Mg calcite (approximately 25–400 m and 600–650  
273 m) and dolomite (300–350 m and 400–600 m) from neomorphism or marine dolomitization of  
274 primary aragonite (Fig. 3) (Shao et al., 2017a). The aragonites or high-Mg calcites (e.g.,  
275 uppermost XK-1 and Jiuzhang A and B cores) are preserved in unlithified carbonate  
276 sands/muds and evaluated as primary precipitates without significant diagenetic alteration,  
277 which is also consistent with an ‘aragonite sea’ in the late Cenozoic (Holland, 2005; Blättler  
278 et al., 2012). Changes in carbonate mineralogy in the XK-1, Jiuzhang A and B drillcores are  
279 also consistent with Sr content variations—distinctly high Sr contents ( $>> 1000$  ppm) support  
280 primary aragonite precipitates in the unconsolidated or weakly consolidated carbonate  
281 sediments in the uppermost XK-1 and Jiuzhang A and B drillcores, and low Sr contents  
282 support diagenetically-originated low-Mg calcite and dolomite deposits in the deeper part of  
283 the XK-1 drillcore (cf. Veizer, 1983; Higgins et al., 2018).

284 The Li contents of inorganic and biogenic carbonates are controlled by multiple factors,



including mineralogy, temperature, pH, solution chemistry and growth rate (Marriott et al., 2004a,b; Fuger et al., 2019; Day et al., 2021; Seyedali et al., 2021). Additionally, the species differences (e.g., foraminifera, brachiopods) influence Li contents of biogenic carbonates (e.g., Dellinger et al., 2018). Regardless of other factors, the mineralogical effects on Li contents are different for inorganic and biogenic carbonates. For inorganic carbonates precipitating under modern seawater-analogous conditions, low-Mg calcites commonly have lower Li contents than aragonites (the partition coefficient of Li:  $K_d^{Li} \sim 0.0025$  to  $0.0035$  for inorganic aragonite;  $K_d^{Li} \sim 0.0005$  to  $0.0020$  for inorganic calcite) (Marriott et al., 2004a,b; Fuger et al., 2019; Seyedali et al., 2021), in contrast to results from biogenic carbonates (i.e., biogenic aragonites generally have lower Li contents than biogenic calcites (Dellinger et al., 2018). Variations in Li and Sr contents of XK-1 and Jiuzhang A and B carbonates can be linked to carbonate mineralogy—mixing of aragonite, high-Mg calcite and low-Mg calcite at depths of 0–25 m with medium Sr contents and high Li contents; low-Mg calcite at depths of 25–400 m and 600–650 m) with relatively low Sr and Li contents; dolomite at depths of 300–350 m and 400–600 m with significantly low Sr but high Li contents (Fig. 5). However, other factors (e.g., pH, solution chemistry, growth rates of carbonate mineral, diagenetic alteration), which highly affect carbonate Li contents, cannot be simply excluded (see discussion below). Particularly, low-Mg calcites in the meteoric zone (25–200 m and 600–650 m depth) have the lowest Li contents of the drillcore, potentially indicative of additional effects (e.g., geochemical compositions of meteoric waters).

Although the Li isotope fractionations during the precipitation of inorganic or biogenic carbonates are not significantly influenced by temperature and salinity (Marriott et al., 2004a,

b; Dellinger et al., 2018), recent experimental studies demonstrate the appreciable effects of pH, solution chemistry and growth rates during synthetic calcite precipitation (Seyedali et al., 2021; Fuger et al., 2022). Under modern seawater-analogous conditions, inorganic carbonates overall exhibit distinct Li isotope compositions for different carbonate minerals (i.e.,  $\Delta^7\text{Li}_{\text{aragonite-seawater}} = -7\text{‰} \sim -12\text{‰}$ ;  $\Delta^7\text{Li}_{\text{calcite-seawater}} = -2\text{‰} \sim -7\text{‰}$ ) (Marriott et al., 2004a,b; Rollion-Bard et al., 2009; Gabitov et al., 2011; Bastian et al., 2018; Pogge von Strandmann et al., 2019; Dellinger et al., 2018, 2020; Seyedali et al., 2021; Fuger et al., 2022). The  $\delta^7\text{Li}$  values of modern shallow-water corals can be slightly lower than inorganic aragonite, indicative of a vital effect during aragonitic skeleton formation (Bastian et al., 2018; Dellinger et al., 2018).

For XK-1 drillcore, the effects of carbonate growth rates and seawater pH can be excluded in this study. Firstly, astronomical tuning of the XK-1 drillcore suggests no significant changes in sedimentation rates from the middle Miocene to the present time (Yi et al., 2018). Despite that the sedimentation rates of carbonate platform may not directly correspond to carbonate growth rates, relatively uniform sedimentation rates of calcites likely imply limited variations of calcite growth rates. Moreover, synthetic calcite experiments show a highly positive correlation between Li isotopic fractionation factors and Li partition coefficients in calcite—low  $\delta^7\text{Li}$  values in step with high Li contents in calcites when fluid compositions are invariant (Fuger et al., 2019, 2022). However, lack of positive correlations between  $\delta^7\text{Li}$  and  $\text{Li}/(\text{Ca}+\text{Mg})$  is observed in the studied calcite samples (Fig. 6A), further supporting that dramatic  $\delta^7\text{Li}$  shifts in the XK-1 drillcore are not dominated by changes in growth rates of carbonates. Additionally, all drillcore carbonates in this study have been

deposited since the middle Miocene (ca. 13–0 Ma), corresponding to a period of time with narrow ranges of surface ocean pH (~8.1–8.3, Sosdian et al., 2018) and seawater chemistry (e.g., Ca concentrations) (Holland, 2005). Taken together,  $\delta^7\text{Li}$  values along with Li contents of the XK-1, Jiuzhang A and B carbonates are more likely determined by mineralogical transitions, early diagenetic regimes and seawater Li isotope compositions from the middle Miocene to the present time.

## 5.2 The $\delta^7\text{Li}$ variations of the XK-1 and Jiuzhang A and B drillcores: combined controls from mineralogy and early diagenetic regimes

The shallow-water corals (aragonitic skeletons) from the South China Sea have lower  $\delta^7\text{Li}$  values ( $17.9\text{‰} \pm 1.0\text{‰}$ ,  $1\sigma$ ) relative to inorganic aragonite (Fig. 4), potentially indicative of species-specific vital effects on Li isotope compositions of corals ( $\Delta^7\text{Li}_{\text{aragonitic coral-inorganic aragonite}} = \sim 2\text{‰}$ ) (Marriott et al., 2004a; Rollion-Bard et al., 2009; Bastian et al., 2018; Dellinger et al., 2018). In contrast, the  $\delta^7\text{Li}$  values of Jiuzhang A and B ( $23.9\text{‰} \pm 0.7\text{‰}$ ,  $1\sigma$ ) and uppermost XK-1 ( $< \sim 25$  m) ( $24.6\text{‰} \pm 1.6\text{‰}$ ,  $1\sigma$ ) are highly uniform and range between those of inorganic aragonite and low-Mg calcite precipitating from modern seawater (Fig. 3), indicative of a mineralogical control on primary carbonate deposits without appreciable species-specific vital effects and early diagenetic alterations (e.g., Pogge von Strandmann et al., 2019; Dellinger et al., 2020). The XK-1 drillcore documents greatly variable  $\delta^7\text{Li}$  values and Li contents, ranging from  $20.2\text{‰}$  to  $30.1\text{‰}$  and from  $0.1\mu\text{g/g}$  to  $1.5\mu\text{g/g}$ , respectively. Previous studies have indicated different diagenetic processes in XK-1, including marine diagenesis from the upper Miocene to Pliocene ( $\sim 200$ – $600$  m) and meteoric–mixing

351 diagenesis in the middle Miocene (~ 580–610 m) and Pleistocene (~ 25–200 m) (Fig. 3),  
 352 marked by low  $\delta^{13}\text{C}$  and  $\delta^{18}\text{O}$  values relative to global seawater records (Shao et al., 2017a).  
 353 Based on age models from foraminiferal biostratigraphy and astronomical tuning (Shao et al.,  
 354 2017b; Yi et al., 2018), the  $\delta^{13}\text{C}$ ,  $\delta^{18}\text{O}$  and  $\delta^7\text{Li}$  records in the XK-1 drillcore are further  
 355 compared to shallow seawater records from the early Miocene to the Pleistocene  
 356 reconstructed from planktonic foraminifera in the South China Sea (Fig. 7) (Cheng et al.,  
 357 2004; Hathorne and James, 2006; Misra and Froelich, 2012). In the middle Miocene and  
 358 Pleistocene, notably negative  $\delta^{13}\text{C}$  and  $\delta^{18}\text{O}$  values of XK-1 carbonates (distinctively lower  
 359 than those of planktonic foraminifers, shallow-water corals and Jiuzhang A and B cores)  
 360 provide clear evidence for prominent meteoric diagenetic alteration of the carbonates in these  
 361 two intervals. The average  $\delta^7\text{Li}$  values of carbonates in these intervals ( $22.4\text{‰} \pm 1.6\text{‰}$ ,  $1\sigma$ )  
 362 are close to those of primary carbonate deposits in the Jiuzhang A and B ( $23.9\text{‰} \pm 0.7\text{‰}$ ,  $1\sigma$ )  
 363 and uppermost XK-1 drillcores ( $24.6\text{‰} \pm 1.6\text{‰}$ ,  $1\sigma$ ), but significantly lower than those of  
 364 foraminifera ( $\Delta^7\text{Li}_{\text{meteoric diagenetic-foram}} = \sim -5\text{‰}$  during the middle Miocene and  $\sim -9\text{‰}$  during  
 365 the Pleistocene) (Figs. 3 and 6C). Despite the changes in seawater  $\delta^7\text{Li}$ , low  $\delta^7\text{Li}$  values in  
 366 these two meteoric zones are similar to modern primary aragonite and high-Mg calcite  
 367 deposits, reflecting, in some sense, a sediment-buffered diagenetic regime. However,  
 368 uniformly low  $\delta^{13}\text{C}$  and  $\delta^{18}\text{O}$  values along with low Li and Sr contents provide robust  
 369 evidence for fluid-buffered meteoric alteration of primary carbonate deposits. Hence, the  
 370 seemingly similar  $\delta^7\text{Li}$  values between meteoric diagenetic calcite and primary aragonite  
 371 suggest that compositions of diagenetic fluids may play a critical role in regulating the  
 372 geochemical signatures of diagenetic calcite (see discussion in 5.4).

Corresponding to a marine diagenetic regime, the  $\delta^7\text{Li}$  curve in XK-1 carbonates from the upper Miocene to Pliocene ( $28.7\text{‰} \pm 0.7\text{‰}$ ,  $1\sigma$ ) is highly consistent with those in foraminifera, showing small and constant offsets ( $\Delta^7\text{Li}_{\text{marine diagenetic-foram}} = \sim -2\text{‰}$ ) (Fig. 7D). Thus, these carbonates potentially document coeval seawater  $\delta^7\text{Li}$  signals that are significantly higher than bulk sediments in the Jiuzhang A and B cores, the Bahamian aragonites and the Atlantic core-top calcitic sediments (Pogge von Strandmann et al., 2019; Dellinger et al., 2020). Significantly higher  $\delta^7\text{Li}$  values of diagenetic calcites relative to primary aragonite and calcite sediments indicate strongly fluid-buffered conditions of marine diagenesis (i.e., seawater-buffered) that shift bulk carbonate  $\delta^7\text{Li}$  to compositions approaching seawater values. Further, despite the distinct Li contents, the  $\delta^7\text{Li}$  values of dolomite and low-Mg calcite samples in this marine diagenetic zone are identical within analytical uncertainty. Accordingly, the Li isotope fractionation of early marine dolomitization is not appreciably different from that of low-Mg calcite deposition, much lower than the values from synthetic dolomite precipitation at high temperatures (150–220°C) that are highly out of ranges of normal seawater conditions (Taylor et al., 2019). The early diagenetic control of  $\delta^7\text{Li}$  variations in the XK-1 drillcore is also supported by clear correlations between  $\delta^7\text{Li}$  and  $\text{Li}/(\text{Ca}+\text{Mg})$ ,  $\text{Mg}/\text{Ca}$ ,  $\delta^{18}\text{O}$ , and  $\delta^{13}\text{C}$  values (Fig. 6). Compared to primary carbonate deposits (aragonite and high-Mg calcite), the meteoric diagenetic carbonates are characterized by low  $\text{Li}/(\text{Ca}+\text{Mg})$ ,  $\delta^7\text{Li}$ ,  $\delta^{18}\text{O}$  and  $\delta^{13}\text{C}$  values, whereas the marine diagenetic carbonates exhibit high  $\text{Li}/(\text{Ca}+\text{Mg})$ ,  $\delta^7\text{Li}$ ,  $\delta^{18}\text{O}$  and  $\delta^{13}\text{C}$ , both of which are determined by compositions of diagenetic fluids (i.e., freshwater or seawater) under fluid-buffered conditions (Fig. 6).

### 5.3 Comparisons of $\delta^7\text{Li}$ signals from the South China Sea and Bahamian shallow-water carbonates

The  $\delta^7\text{Li}$  and Li contents in the XK-1 drillcore are further compared to those of the Bahamian carbonates (Clino, Unda and Site 1007 cores) that have been investigated for Li isotopes and Li/(Ca+Mg) ratios (Dellinger et al., 2020). Shallow-water carbonates from the South China Sea and the Bahamas exhibit coherent changes in  $\delta^7\text{Li}$  and Li/(Ca+Mg) from the Pliocene to the Pleistocene (Fig. 8), implying globally correlative Li isotope signals controlled by early diagenetic regimes corresponding to global climate and sea-level changes.

Despite the widely separated locations of XK-1 and the Bahamian Clino and Unda drillcores, the  $\delta^7\text{Li}$  values of meteoric carbonates in these cores are highly uniform ( $\delta^7\text{Li}_{\text{XK-1}} = 22.4\text{‰} \pm 1.6\text{‰}$  and  $\delta^7\text{Li}_{\text{Bahamas}} = 22.1\text{‰} \pm 3.0\text{‰}$ ,  $1\sigma$ ), similar to primary carbonate deposits in the South China Sea and the Bahamas (cf. Dellinger et al., 2020). Given significantly low  $\delta^{13}\text{C}$  and  $\delta^{18}\text{O}$  in meteoric zones, a meteoric fluid-buffered diagenetic regime can be identified in Clino, Unda and XK-1 drillcores (Dellinger et al., 2020 and this study). Observations of similar  $\delta^7\text{Li}$  values of meteoric and primary carbonates are interpreted as a coincidental event in the Bahamas (Dellinger et al., 2020). However, highly uniform  $\delta^7\text{Li}$  records in the South China Sea and the Bahamas may provide more insights into the evaluation of meteoric alteration of  $\delta^7\text{Li}$  signals. Two potential hypotheses may account for similar  $\delta^7\text{Li}$  signals in meteoric calcite and primary aragonite/high-Mg calcite—(1)  $\delta^7\text{Li}$  values of freshwater (i.e., river water or groundwater) are close to those of primary carbonate sediments; (2) a sediment-buffered condition for Li isotope during the meteoric diagenesis. The first hypothesis could work for modern shallow-water carbonates as modern river water and groundwater export to

417 the ocean may have similar average  $\delta^7\text{Li}$  values ( $\sim 23\text{‰}$ ) (Huh et al., 1998; Murphy et al.,  
 418 2019; Mayfield et al., 2021), close to those of primary carbonate sediments precipitating from  
 419 seawater with modern ocean  $\delta^7\text{Li}$  ( $23.7 \pm 0.9$ ,  $1\sigma$ ) (Fig. 9). However, large variations and  
 420 heterogeneities of riverine and groundwater  $\delta^7\text{Li}$  have been demonstrated in previous studies  
 421 (Huh et al., 1998; Négrel et al., 2010, 2012; Lemarchand et al., 2010; Pogge von Strandmann  
 422 et al., et al., 2014), challenging the reliability of this hypothesis. Accordingly, it may not be  
 423 easy to justify that the South China Sea and Bahamas share the similar Li isotope  
 424 compositions of freshwater, since these two regions are widely separated with different  
 425 latitudes and weathering intensities. Instead, we suggest that sediment-buffered conditions for  
 426 Li isotope system during the meteoric diagenesis would be responsible for the similar  $\delta^7\text{Li}$   
 427 values of meteoric carbonates in the South China Sea and the Bahamas. In general, Li  
 428 concentrations of freshwater are significantly lower than that of seawater (e.g., for modern  
 429 Earth,  $[\text{Li}]_{\text{rivers}} = \sim 1.5 \text{ ng/mL}$ ,  $[\text{Li}]_{\text{seawater}} = \sim 180 \text{ ng/mL}$ ) (Huh et al., 1998). Thus, meteoric  
 430 diagenesis (water-rock interaction) is more likely to induce sediment-buffered  $\delta^7\text{Li}$  signals  
 431 relative to marine diagenesis (Banner and Hanson, 1990; Ahm et al., 2018; Zhao et al., 2020;  
 432 Fantle et al., 2020). Moreover, meteoric water flowing through shallow-water carbonate  
 433 platforms (e.g., the Great Bahama Bank and South China Sea reef carbonate platforms)  
 434 potentially has even lower Li concentrations than terrestrial river water or groundwater,  
 435 facilitating the inheritance of original  $\delta^7\text{Li}$  signals from primary carbonate deposits. This  
 436 interpretation is supported by significantly lower Li contents of meteoric carbonates ( $4.7 \pm 1.5$   
 437  $\mu\text{mol/mol}$ ,  $1\sigma$ ) than those of primary carbonates ( $19.17 \pm 8.37 \mu\text{mol/mol}$ ,  $1\sigma$ ) and marine  
 438 diagenetic carbonates ( $13.81 \pm 3.38 \mu\text{mol/mol}$ ,  $1\sigma$ ) in the South China Sea and the Bahamas

(Fig. 8). In contrast, most marine diagenetic carbonates (both dolomite and low-Mg calcite), which effectively archive ambient seawater compositions with notably high Li contents, denote a seawater-buffered diagenetic regime for shallow-marine carbonates in this study and Dellinger et al. (2020). Further, highly consistent  $\delta^7\text{Li}$  trends in the late Cenozoic built from marine dolostone and foraminifera argue for the potential of (syn)sedimentary dolostone as an archive for Precambrian seawater Li isotope signals (cf. Crockford et al., 2020). In conclusion, the Li records of shallow-water carbonates in the South China Sea and the Bahamas can be well correlated, and the  $\delta^7\text{Li}$  variations within each drillcore are related to changes in early diagenetic regimes.

#### 5.4 Evaluation of shallow-water carbonate as an archive for Li isotope compositions of ancient seawater

Early diagenesis (both meteoric and marine diagenesis) has been widely proposed to significantly overprint the primary geochemical signature of shallow-water carbonates (Stewart et al., 2015; Hardisty et al., 2017; Chen et al., 2018; Higgins et al., 2018; Dellinger et al., 2020), hampering the use of geochemical indices archived by ancient carbonates to reconstruct the paleo-environmental evolution. However, to date, most of the research has concentrated on shallow-water carbonates from the Great Bahama Bank, and global comparisons are lacking. This study reports new Li isotope data from the XK-1 drillcore, the South China Sea, which provides a case study of ca. 13 million-year diagenetic history for shallow-water carbonates. Highly consistent trends of  $\delta^7\text{Li}$  and Li contents in the South China Sea and the Bahamas provide robust evidence for an early diagenetic control on Li isotope



records in shallow-water carbonates from the Pliocene to Pleistocene. This observation highlights that the early diagenetic alteration of shallow-water carbonates can be globally correlative on both spatial and temporal scales. The Li isotope compositions of shallow-water carbonates are closely related to carbonate mineralogy, seawater chemistry and early diagenetic regimes (Dellinger et al., 2018, 2020; Pogge von Strandmann et al., 2019).

The  $\delta^7\text{Li}$  data of bulk inorganic carbonates from the latest Miocene are further compiled in Fig. 9 ( $\delta^7\text{Li}$  of the global ocean during this period is relatively constant and equal to the modern seawater value) (Pogge von Strandmann et al., 2019; Dellinger et al., 2020; this study). We find that marine diagenetic carbonates, including low-Mg calcite and dolomite with normal marine  $\delta^{18}\text{O}$  and  $\delta^{13}\text{C}$  signals, have  $\delta^7\text{Li}$  values of  $29.2 \pm 1.4$  ( $1\sigma$ ) approaching modern seawater Li isotope compositions ( $\Delta^7\text{Li}_{\text{marine diagenetic-seawater}} = -1.5\text{‰}$ ). In contrast, in step with significantly negative  $\delta^{18}\text{O}$  and  $\delta^{13}\text{C}$  values,  $\delta^7\text{Li}$  values of meteoric diagenetic carbonates ( $22.6 \pm 2.4$ ,  $1\sigma$ ) are significantly lower than those of ambient seawater ( $\Delta^7\text{Li}_{\text{meteoric diagenetic-seawater}} = -8.0\text{‰}$ ) but interestingly close to those of primary carbonate deposits (i.e., mixing of aragonite and high-Mg calcite) ( $23.7 \pm 0.9$ ,  $1\sigma$  and average  $\Delta^7\text{Li}_{\text{primary-seawater}} = -7.0\text{‰}$ ). The Li isotopic behavior during meteoric diagenesis appears opposite to many other isotope systems (e.g.,  $\delta^{13}\text{C}$ ,  $\delta^{18}\text{O}$ ,  $\delta^{11}\text{B}$ ,  $\delta^{238}\text{U}$ ), whose compositions have been notably altered during the meteoric diagenesis. (Melim et al., 2002; Stewart et al., 2015; Chen et al., 2018). Further, meteoric diagenetic carbonates are characterized by appreciably low  $\text{Li}/(\text{Ca}+\text{Mg})$  ( $\sim 5 \mu\text{mol/mol}$ ) relative to marine diagenetic carbonates ( $10\text{--}20 \mu\text{mol/mol}$ ). As mentioned above, we suggest that compositional differences between seawater and meteoric water may have played a first-order control on  $\delta^7\text{Li}$  and Li content of diagenetic low-Mg calcites, as seawater

generally has average Li concentrations ~ 100 times higher than freshwater (river or groundwater) (average  $[\text{Li}]_{\text{seawater}} = \sim 180 \text{ ng/mL}$ ; average  $[\text{Li}]_{\text{river}} = \sim 1.5 \text{ ng/mL}$  ranging from 0.21 ng/mL to 14 ng/mL) (Huh et al., 1998). Given low Li contents in inorganic carbonate minerals ( $K_d^{\text{Li}} = 0.0005\text{--}0.0020$  for low-Mg calcite,  $0.0025\text{--}0.0035$  for aragonite) (Marriott et al., 2004a,b; Fuger et al., 2019; Seyedali et al., 2021), the Li isotope system in marine carbonates is susceptible to early diagenetic alteration. However, Li concentrations and isotopes of diagenetic fluids would ultimately dominate the regimes of early diagenesis (i.e., fluid-buffered or sediment-buffered) and thus  $\delta^7\text{Li}$  values of diagenetic carbonates. Further, a numerical model of early diagenesis following Ahm et al. (2018) is used to evaluate the effects of fluid compositions on diagenetic regimes and carbonate Li isotopes. Based on the baseline of modeling inputs for the Bahamian carbonates (all the parameters are shown in Table 1), we reproduce  $\delta^7\text{Li}$  changes within the sediment piles during the transition from primary aragonite to diagenetic low-Mg calcite, following interactions between primary minerals and diagenetic fluids (i.e., seawater and freshwater) (Fig. 10A, B). The Li isotope fractionation during the carbonate diagenesis has not been constrained yet, nevertheless, low-Mg calcites after early marine diagenesis in the Bahamas (Dellinger et al., 2020; Murphy et al., 2022) and South China Sea (this study) show limited Li isotope offsets relative to ambient seawater. Hence, we suggest a value of 0.999 as Li isotope fractionation factor used in the diagenetic model. This value is lower than that for calcite precipitation in laboratory experiments and natural environment (Marriott et al., 2004; Dellinger et al., 2018; Pogge von Strandmann et al., 2019; Day et al., 2021) likely due to much slower dissolution-precipitation rates than calcite precipitation in the laboratory conditions, but consistent with

505 Ca isotope fractionation factor ( $\sim 1.000$ ) during the carbonate diagenesis (Fantle and  
 506 DePaolo, 2007; Jacobson and Holmden, 2008; Fantle and Higgins, 2014; Higgins et al., 2018,  
 507 Ahm et al., 2018). Using a value of 0.999 for the Li isotope fractionation factor and a  $K_d^{Li}$   
 508 value of 0.001 for low-Mg calcite and 0.002 for dolomite (experimental constraints on the  
 509  $K_d^{Li}$  for dolomite are absent but we, herein, assume a higher value relative to low-Mg  
 510 calcite), we run the diagenetic model with different compositions of diagenetic fluids. Under  
 511 modern seawater conditions assumed for early marine diagenesis ( $[Li]_{seawater} = 0.18 \mu\text{g/mL}$ ,  
 512  $[Ca]_{seawater} = 410 \mu\text{g/mL}$ ) (e.g., Chester and Jickells, 2012; Misra and Froelich, 2012), the  
 513 overall sediment piles are marked by a strongly fluid-buffered diagenetic regime for the Li  
 514 isotope system, suggesting that the diagenetic carbonates ultimately document the Li isotope  
 515 compositions of seawater (i.e., low-Mg calcites and dolomites in the South China Sea and the  
 516 Bahamas). When applying lower Li concentrations of the diagenetic fluids to the model, the  
 517 deeper sediments gradually change to a relatively sediment-buffered diagenetic regime (Fig.  
 518 10A). Under modern river/groundwater conditions assumed for meteoric diagenesis  
 519 ( $[Li]_{freshwater} = 0.0015 \mu\text{g/mL}$ ,  $[Ca]_{freshwater} = 82 \mu\text{g/mL}$ ) (Chester and Jickells, 2012; Huh et al.,  
 520 1998), changes in  $\delta^7\text{Li}$  of the diagenetic carbonates are similar to those under seawater  
 521 analogous conditions with significantly lower Li concentrations (Fig. 10B). We also model  
 522 correlations between  $\delta^7\text{Li}$  and  $\text{Mg/Ca}$ ,  $\delta^{18}\text{O}$ ,  $\delta^{13}\text{C}$  values in the processes of marine  
 523 dolomitization, marine neomorphism and meteoric diagenesis, denoting the mineralogical  
 524 transitions from primary aragonite/high-Mg calcite to marine dolomite, marine low-Mg  
 525 calcite and meteoric low-Mg calcite, respectively. The modeling results can overall reproduce  
 526 the trends in  $\delta^7\text{Li}$  and  $\text{Mg/Ca}$ ,  $\delta^{18}\text{O}$  and  $\delta^{13}\text{C}$  of the bulk carbonates in the South China Sea

during different diagenetic regimes (Fig. 10C, D, E, F).

The inheritance of primary  $\delta^7\text{Li}$  signals in meteoric diagenetic calcites is also consistent with the pristine records of  $^{87}\text{Sr}/^{86}\text{Sr}$ ,  $\delta^{34}\text{S}$  of carbonate associated sulfate, and Ce anomaly in other meteoric diagenetic carbonates (Gill et al., 2008; Liu et al., 2019; Fan et al., 2019). Low water-rock ratios of these elements during the meteoric diagenesis may have facilitated the preservation of primary compositions in carbonates, supported by results from previous diagenetic models (Banner and Hanson, 1990; Ahm et al., 2018; Fantle et al., 2020; Zhao et al., 2020). This observation suggests that meteoric diagenesis may not always overprint the geochemical signature of primary carbonate minerals. The differences in isotopic behavior during the early diagenesis of shallow-water carbonates are caused by the effects of carbonate mineralogy and diagenetic fluid compositions on different isotope systems. For Li isotopes, the mineralogy and aquatic chemistry may dominate the  $\delta^7\text{Li}$  signals in primary carbonate deposits, whereas marine diagenesis can completely overprint the primary  $\delta^7\text{Li}$  signals and shift them toward ambient seawater compositions (i.e., fluid-buffered conditions) due to high Li concentrations of seawater, which highlights the potential use of shallow-water carbonate as a snapshot of coeval seawater Li isotope compositions. This observation can provide more support for using inorganic bulk carbonates, especially dolostones, to reconstruct seawater  $\delta^7\text{Li}$  evolution in deep time (cf. Crockford et al., 2020; Kalderon-Asael et al., 2021). Given significantly lower Li concentrations in freshwater relative to seawater, meteoric diagenesis may have not notably shifted  $\delta^7\text{Li}$  values of primary carbonates (i.e., sediment-buffered conditions). Additionally, similar  $\delta^7\text{Li}$  values of Neogene diagenetic carbonates (low-Mg calcites) and coeval seawater in the South China Sea and the Bahamas imply little or limited

Li isotope fractionations during the early diagenesis.

A full consideration of potential offsets is required when using carbonates that experience different types of early diagenesis to reconstruct coeval seawater information (cf. Dellinger et al., 2020; Murphy et al., 2022). Despite other effects on carbonate Li contents, relationships between  $\text{Li}/(\text{Ca}+\text{Mg})$  and  $\delta^7\text{Li}$  values can be used to constrain the diagenetic regimes of shallow-water carbonates. Primary carbonate deposits (mixing of primary aragonite, high-Mg calcite and low-Mg calcite) overall have variable but high  $\text{Li}/(\text{Ca}+\text{Mg})$  ( $19.2 \pm 10.4 \mu\text{mol/mol}$ ), and significantly lower  $\delta^7\text{Li}$  relative to modern seawater ( $\Delta^7\text{Li}_{\text{primary-seawater}} = -7.0\text{‰}$  on average). By contrast, marine diagenetic carbonates (limestone and dolostone) have slightly lower  $\text{Li}/(\text{Ca}+\text{Mg})$  ( $13.8 \pm 3.4 \mu\text{mol/mol}$ ) but similar  $\delta^7\text{Li}$  to modern seawater ( $\Delta^7\text{Li}_{\text{primary-seawater}} = -1.5\text{‰}$  on average). Meteoric diagenetic carbonates show distinctly low  $\text{Li}/(\text{Ca}+\text{Mg})$  ( $4.7 \pm 1.5 \mu\text{mol/mol}$ ) and much lower  $\delta^7\text{Li}$  relative to modern seawater ( $\Delta^7\text{Li}_{\text{primary-seawater}} = -8.5\text{‰}$  on average). Additionally, co-analyses of other isotope systems (e.g., C, O, Ca, Mg isotopes) (e.g., Murphy et al., 2022) also help to better constrain the diagenetic regimes and compositions of diagenetic fluids for ancient carbonate  $\delta^7\text{Li}$  records.

## 6. Conclusions

New Li isotope measurements along with trace elemental data of shallow-water carbonates from the South China Sea are reported to better constrain the carbonate mineralogical and diagenetic controls on Li isotope compositions of bulk inorganic carbonates. Carbonates from two shallow drillcores (Jiuzhang A and B) and the uppermost part of a deep drillcore (XK-1), which represent primary carbonate deposits, have average

571  $\delta^7\text{Li}$  values of  $24.6\text{‰} \pm 1.6\text{‰}$  ( $1\sigma$ ) ( $\Delta^7\text{Li}_{\text{carbonate-seawater}} = \sim -6.0\text{‰}$ ) , indicative of the primary  
 572 deposits of aragonite and high-Mg calcite. By contrast, marine diagenetic carbonates,  
 573 including low-Mg calcite and dolomite in the XK-1 drillcore show  $\delta^7\text{Li}$  values of  $28.7\text{‰} \pm$   
 574  $0.7\text{‰}$  ( $1\sigma$ ) ( $\Delta^7\text{Li}_{\text{carbonate-seawater}} = \sim -2.0\text{‰}$ ), significantly higher than those of primary  
 575 carbonate deposits but close to ambient seawater. Small and constant  $\delta^7\text{Li}$  offsets between  
 576 marine diagenetic carbonates and seawater highlight a strongly fluid-buffered diagenetic  
 577 regime for shallow-marine carbonates. For meteoric diagenetic carbonates from the lowest  
 578 and upper parts of the XK-1 drillcore, their  $\delta^7\text{Li}$  values ( $22.4\text{‰} \pm 1.6\text{‰}$ ,  $1\sigma$ ) are significantly  
 579 lower than seawater values ( $\Delta^7\text{Li}_{\text{carbonate-seawater}} = \sim -8.0\text{‰}$ ) but very close to those of primary  
 580 inorganic carbonate deposits. This observation is attributed to relatively sediment-buffered  
 581 conditions for meteoric diagenesis potentially due to significantly low Li concentrations and  
 582  $\delta^7\text{Li}$  values of freshwater relative to modern seawater. Further, the  $\delta^7\text{Li}$  records in the XK-1  
 583 drillcore (South China Sea) are highly consistent with those in the Clino and Unda drillcores  
 584 (Great Bahama Bank), providing robust evidence for a globally correlative diagenetic history  
 585 of shallow-water carbonates from the Neogene. Such observations suggest that the early  
 586 diagenesis of shallow-water carbonates are not individual events, and would have been  
 587 ubiquitous in ancient records. The early diagenetic alteration, including marine and meteoric  
 588 diagenesis, does not hamper the use of inorganic carbonates as a recorder for seawater  $\delta^7\text{Li}$ . In  
 589 particular, given that marine diagenetic carbonates show  $\delta^7\text{Li}$  values very close to ambient  
 590 seawater, ancient marine limestones and dolostones are likely to be suitable targets for  
 591 research on the reconstruction of ancient seawater  $\delta^7\text{Li}$ . Given different sensitivities of isotope  
 592 systems during early diagenesis, it is better to evaluate the diagenetic effects on compositions

of shallow-water carbonates on a case-by-case basis. Different diagenetic regimes (marine diagenesis vs. meteoric diagenesis, fluid-buffered vs. sediment-buffered conditions) should also be individually considered when using shallow-water carbonates as paleo-seawater archives.

## Acknowledgments

This work was funded by National Key Research and Development Program of China (2021YFA0718100, 2021YFC3100603); the National Natural Science Foundation of China (42002002, 42073002), the Strategic Priority Research Program(B) of the Chinese Academy of Sciences (XDB26000000); Fundamental Research Funds for Central Universities (14380125, 14380168), and Frontiers Science Center for Critical Earth Material Cycling Fund (DLTD2102); Philip A. E. Pogge von Strandmann acknowledges support from an ERC grant (682760).

## Appendix A. Supplementary Material

Supplementary material to this article mainly includes research data and detailed descriptions of analytical method and diagenetic model.

## References

Ahm A.-S. C., Bjerrum C. J., Blättler C. L., Swart P. K. and Higgins J. A. (2018) Quantifying early marine diagenesis in shallow-water carbonate sediments. *Geochim. Cosmochim. Acta* **236**, 140-159.

615 Andrews E., Pogge von Strandmann P. A. E. and Fantle M. S. (2020) Exploring the importance  
 616 of authigenic clay formation in the global Li cycle. *Geochim. Cosmochim. Acta* **289**, 47-  
 617 68.  
 618 Banner J. L. (1995) Application of the trace element and isotope geochemistry of strontium to  
 619 studies of carbonate diagenesis. *Sedimentology* **42**, 805-824.  
 620 Banner J. L. and Hanson G. N. (1990) Calculation of simultaneous isotopic and trace element  
 621 variations during water-rock interaction with applications to carbonate diagenesis,  
 622 *Geochim. Cosmochim. Acta* **54**, 3123-3137.  
 623 Bastian L., Vigier N., Reynaud S., Kerros M.-E., Revel M. and Bayon G. (2018) Lithium  
 624 Isotope Composition of Marine Biogenic Carbonates and Related Reference Materials.  
 625 *Geostand. Geoanal. Res.* **42**, 403-415.  
 626 Blättler C. L., Henderson G. M. and Jenkyns H. C. (2012) Explaining the Phanerozoic Ca  
 627 isotope history of seawater. *Geology* **40**, 843-846.  
 628 Chen X., Romaniello S. J., Herrmann A. D., Hardisty D., Gill B. C. and Anbar A. D. (2018)  
 629 Diagenetic effects on uranium isotope fractionation in carbonate sediments from the  
 630 Bahamas. *Geochim. Cosmochim. Acta* **237**, 294-311.  
 631 Cheng X., Zhao Q., Wang J., Jian Z., Xia P., Huang B., Fang D., Xu J., Zhou Z., and Wang P.  
 632 (2004) Data report: Stable Isotopes from Sites 1147 and 1148. In Prell, W.L., Wang, P.,  
 633 Blum, P., Rea, D.K., and Clemens, S.C. (Eds.), *Proc. ODP, Sci. Results*, **184**, 1–12.  
 634 Available from World Wide Web: <[http://www-odp.tamu.edu/](http://www-odp.tamu.edu/publications/184_SR/VOLUME/CHAPTERS/223.PDF)  
 635 [publications/184\\_SR/VOLUME/CHAPTERS/223.PDF](http://www-odp.tamu.edu/publications/184_SR/VOLUME/CHAPTERS/223.PDF)>.  
 636 Chester R. and Jickells T. Marine geochemistry. 3rd Edition, John Wiley & Sons, 2012; p. 411.



- 637 Craig H. (1953) The geochemistry of the stable carbon isotopes. *Geochim. Cosmochim. Acta* **3**,  
638 53–92.
- 639 Crockford P. W., Kunzmann M., Blättler C. L., Kalderon-Asael B., Murphy J. G., Ahm A.-S.,  
640 Sharoni S., Halverson G. P., Planavsky N. J., Halevy I. and Higgins J. A. (2020)  
641 Reconstructing Neoproterozoic seawater chemistry from early diagenetic dolomite.  
642 *Geology* **49**, 442-446.
- 643 Day C. C., von Strandmann P. A. E. P. and Mason A. J. (2021) Lithium isotopes and partition  
644 coefficients in inorganic carbonates: Proxy calibration for weathering reconstruction.  
645 *Geochim. Cosmochim. Acta* **305**, 243-262.
- 646 Dellinger M., Gaillardet J., Bouchez J., Calmels D., Louvat P., Dosseto A., Gorge C., Alanoca  
647 L. and Maurice L. (2015) Riverine Li isotope fractionation in the Amazon River basin  
648 controlled by the weathering regimes. *Geochim. Cosmochim. Acta* **164**, 71-93.
- 649 Dellinger M., Hardisty D. S., Planavsky N. J., Gill B. C., Kalderon-Asael B., Asael D.,  
650 Croissant T., Swart P. K. and West A. J. (2020) The effects of diagenesis on lithium isotope  
651 ratios of shallow marine carbonates. *Am. J. Sci.* **320**, 150-184.
- 652 Dellinger M., West A. J., Paris G., Adkins J. F., Pogge von Strandmann P. A. E., Ullmann C. V.,  
653 Eagle R. A., Freitas P., Bagard M.-L., Ries J. B., Corsetti F. A., Perez-Huerta A. and Kampf  
654 A. R. (2018) The Li isotope composition of marine biogenic carbonates: Patterns and  
655 mechanisms. *Geochim. Cosmochim. Acta* **236**, 315-335.
- 656 Emrich K., Ehhalt D. H. and Vogel J. C. (1970) Carbon isotope fractionation during the  
657 precipitation of calcium carbonate. *Earth Planet. Sci. Lett.* **8**, 363-371.
- 658 Föger A., Konrad F., Leis A., Dietzel M. and Mavromatis V. (2019) Effect of growth rate and

659 pH on lithium incorporation in calcite. *Geochim. Cosmochim. Acta* **248**, 14-24.

660 Füger A., Kuessner M., Rollion-Bard C., Leis A., Magna T., Dietzel M. and Mavromatis V.

661 (2022) Effect of growth rate and pH on Li isotope fractionation during its incorporation in

662 calcite. *Geochim. Cosmochim. Acta* **323**, 276-290.

663 Fan T., Yu K., Zhao J., Jiang W., Xu S., Zhang Y., Wang R., Wang Y., Feng Y., Bian L., Qian H.

664 and Liao W. (2019) Strontium isotope stratigraphy and paleomagnetic age constraints on

665 the evolution history of coral reef islands, northern South China Sea. *GSA Bulletin* **132**,

666 803-816.

667 Fantle M. S., Barnes B. D. and Lau K. V. (2020) The Role of Diagenesis in Shaping the

668 Geochemistry of the Marine Carbonate Record. *Annu. Rev. Earth Planet. Sci.* **48**, 549-583.

669 Fantle M. S. and DePaolo D. J. (2007) Ca isotopes in carbonate sediment and pore fluid from

670 ODP Site 807A: The  $\text{Ca}^{2+}(\text{aq})$ -calcite equilibrium fractionation factor and calcite

671 recrystallization rates in Pleistocene sediments. *Geochim. Cosmochim. Acta* **71**, 2524-

672 2546.

673 Fantle M. S. and Higgins J. (2014) The effects of diagenesis and dolomitization on Ca and Mg

674 isotopes in marine platform carbonates: Implications for the geochemical cycles of Ca and

675 Mg. *Geochim. Cosmochim. Acta* **142**, 458-481.

676 Gabitov R. I., Schmitt A. K., Rosner M., McKeegan K. D., Gaetani G. A., Cohen A. L., Watson

677 E. B. and Harrison T. M. (2011) In situ  $\delta^7\text{Li}$ , Li/Ca, and Mg/Ca analyses of synthetic

678 aragonites. *Geochem. Geophys. Geosyst.* **12**, Q03001.

679 Gill B. C., Lyons T. W. and Frank T. D. (2008) Behavior of carbonate-associated sulfate during

680 meteoric diagenesis and implications for the sulfur isotope paleoproxy. *Geochim.*

681 *Cosmochim. Acta* **72**, 4699-4711.

682 Hardisty D. S., Lu Z., Bekker A., Diamond C. W., Gill B. C., Jiang G., Kah L. C., Knoll A. H.,  
683 Loyd S. J., Osburn M. R., Planavsky N. J., Wang C., Zhou X. and Lyons T. W. (2017)  
684 Perspectives on Proterozoic surface ocean redox from iodine contents in ancient and recent  
685 carbonate. *Earth Planet. Sci. Lett.* **463**, 159-170.

686 Hathorne E. and James R. (2006) Temporal record of lithium in seawater: A tracer for silicate  
687 weathering? *Earth Planet. Sci. Lett.* **246**, 393-406.

688 Higgins J. A., Blättler C. L., Lundstrom E. A., Santiago-Ramos D. P., Akhtar A. A., Ahm A.-S.  
689 C., Bialik O., Holmden C., Bradbury H., Murray S. T. and Swart P. K. (2018) Mineralogy,  
690 early marine diagenesis, and the chemistry of shallow-water carbonate sediments.  
691 *Geochim. Cosmochim. Acta* **220**, 512-534.

692 Holland H. D. (2005) Sea level, sediments and the composition of seawater. *Am. J. Sci.* **305**,  
693 220-239.

694 Huh Y., Chan L.-H., Zhang L. and Edmond J. M. (1998) Lithium and its isotopes in major world  
695 rivers: implications for weathering and the oceanic budget. *Geochim. Cosmochim. Acta*  
696 **62**, 2039-2051.

697 Jacobson A. D. and Holmden C. (2008)  $\delta^{44}\text{Ca}$  evolution in a carbonate aquifer and its bearing  
698 on the equilibrium isotope fractionation factor for calcite. *Earth Planet. Sci. Lett.* **270**,  
699 349-353.

700 Kalderon-Asael B., Katchinoff J. A. R., Planavsky N. J., Hood A. v.S., Dellinger M., Bellefroid  
701 E. J., Jones D. S., Hofmann A., Ossa F. O., Macdonald F. A., Wang C., Isson T. T., Murphy  
702 J. G., Higgins J. A., West A. J., Wallace M. W., Asael D. and Pogge von Strandmann P. A.

703 E. (2021) A lithium-isotope perspective on the evolution of carbon and silicon cycles.  
 704 *Nature* **595**, 394-398.

705 Kim S.-T., Mucci A. and Taylor B. E. (2007) Phosphoric acid fractionation factors for calcite  
 706 and aragonite between 25 and 75 °C: Revisited. *Chem. Geol.* **246**, 135-146.

707 Lécuyer C. (2016) Seawater residence times of some elements of geochemical interest and the  
 708 salinity of the oceans. *Bull. Soc. Geol. Fr.* **187**, 245-260.

709 Lechler M., Pogge von Strandmann P. A. E., Jenkyns H. C., Prosser G. and Parente M. (2015)  
 710 Lithium-isotope evidence for enhanced silicate weathering during OAE 1a (Early Aptian  
 711 Selli event). *Earth Planet. Sci. Lett.* **432**, 210-222.

712 Lemarchand, E., Chabaux, F., Vigier, N., Millot, R. and Pierret, M.-C. (2010) Lithium isotope  
 713 systematics in a forested granitic catchment (Strengbach, Vosges Mountains, France).  
 714 *Geochim. Cosmochim. Acta* **74**, 4612-4628.

715 Liu X.-M., Hardisty D. S., Lyons T. W. and Swart P. K. (2019) Evaluating the fidelity of the  
 716 cerium paleoredox tracer during variable carbonate diagenesis on the Great Bahamas Bank.  
 717 *Geochim. Cosmochim. Acta* **248**, 25-42.

718 Marriott C. S., Henderson G. M., Belshaw N. S. and Tudhope A. W. (2004a) Temperature  
 719 dependence of  $\delta^7\text{Li}$ ,  $\delta^{44}\text{Ca}$  and Li/Ca during growth of calcium carbonate. *Earth Planet.*  
 720 *Sci. Lett.* **222**, 615-624.

721 Marriott C. S., Henderson G. M., Crompton R., Staubwasser M. and Shaw S. (2004b) Effect of  
 722 mineralogy, salinity, and temperature on Li/Ca and Li isotope composition of calcium  
 723 carbonate. *Chem. Geol.* **212**, 5-15.

724 Mayfield K. K., Eisenhauer A., Santiago Ramos D. P., Higgins J. A., Horner T. J., Auro M.,

725 Magna T., Moosdorf N., Charette M. A., Gonneea M. E., Brady C. E., Komar N., Peucker-  
 726 Ehrenbrink B. and Paytan A. (2021) Groundwater discharge impacts marine isotope  
 727 budgets of Li, Mg, Ca, Sr, and Ba. *Nat. Commun.* **12**, 148.

728 McCrea J. M. (1950) Isotopic chemistry of carbonates and a paleo-temperature scale. *J. Chem.*  
 729 *Phys.* **18**, 849–857.

730 Melim L. A., Westphal H., Swart P. K., Eberli G. P., Munnecke A. (2002) Questioning carbonate  
 731 diagenetic paradigms: evidence from the Neogene of the Bahamas. *Mar. Geol.* **185**, 27-53.

732 Millot R., Guerrot C. and Vigier N. (2004) Accurate and High-Precision Measurement of  
 733 Lithium Isotopes in Two Reference Materials by MC-ICP-MS. *Geostand. Geoanal. Res.*  
 734 **28**, 153-159.

735 Millot R., Vigier N. and Gaillardet J. (2010) Behaviour of lithium and its isotopes during  
 736 weathering in the Mackenzie Basin, Canada. *Geochim. Cosmochim. Acta* **74**, 3897-3912.

737 Misra S. and Froelich P. N. (2012) Lithium isotope History of Cenozoic Seawater: Changes in  
 738 Silicate Weathering and Reverse Weathering. *Science* **335**, 818-823.

739 Murphy, J.G., Ahm, A.-S.C., Swart, P.K. and Higgins, J.A. (2022) Reconstructing the lithium  
 740 isotopic composition ( $\delta^7\text{Li}$ ) of seawater from shallow marine carbonate sediments.  
 741 *Geochim. Cosmochim. Acta* **337**, 140-154.

742 Murphy M. J., Porcelli D., Pogge von Strandmann P. A. E., Hirst C. A., Kutscher L., Katchinoff  
 743 J. A., Mörrh C.-M., Maximov T. and Andersson P. S. (2019) Tracing silicate weathering  
 744 processes in the permafrost-dominated Lena River watershed using lithium isotopes.  
 745 *Geochim. Cosmochim. Acta* **245**, 154-171.

746 Négrel, P., Millot, R., Brenot, A. and Bertin, C. (2010) Lithium isotopes as tracers of

747 groundwater circulation in a peat land. *Chem. Geol.* **276**, 119-127.

748 Négrel, P., Millot, R., Guerrot, C., Petelet-Giraud, E., Brenot, A. and Malcuit, E. (2012)

749 Heterogeneities and interconnections in groundwaters: Coupled B, Li and stable-isotope

750 variations in a large aquifer system (Eocene Sand aquifer, Southwestern France). *Chem.*

751 *Geol.* **296-297**, 83-95.

752 O'Neil J. R., Clayton R. N. and Mayeda T. K. (1969) Oxygen Isotope Fractionation in Divalent

753 Metal Carbonates. *J.chem.phys.* **51**, 5547-5558.

754 Penniston-Dorland S., Liu X.-M., Rudnick R. L. (2017) Lithium Isotope Geochemistry. *Rev.*

755 *Mineral. Geochem.* **82**, 165-217.

756 Pogge von Strandmann P. A. E., Burton K. W., James R. H., van Calsteren P., Gíslason S. R.

757 and Mokadem F. (2006) Riverine behaviour of uranium and lithium isotopes in an actively

758 glaciated basaltic terrain. *Earth Planet. Sci. Lett.* **251**, 134-147.

759 Pogge von Strandmann P. A. E., Dellinger M. and West A. J. (2021a) Lithium Isotopes. In

760 *Geochemical Tracers in Earth System Science* (eds. T. Lyons, A. Turchyn and C. Reinhard).

761 Cambridge University Press.

762 Pogge von Strandmann P. A. E., Desrochers A., Murphy M. J., Finlay A. J., Selby D. and Lenton

763 T. M. (2017a) Global climate stabilisation by chemical weathering during the Hirnantian

764 glaciation. *Geochem. Perspect. Lett.* **3**, 230-237.

765 Pogge von Strandmann P. A. E., Frings P. J. and Murphy M. J. (2017b) Lithium isotope

766 behaviour during weathering in the Ganges Alluvial Plain. *Geochim. Cosmochim. Acta*

767 **198**, 17-31.

768 Pogge von Strandmann P. A. E., Jenkyns H. C. and Woodfine R. G. (2013) Lithium isotope

769 evidence for enhanced weathering during Oceanic Anoxic Event 2. *Nat. Geosci.* **6**, 668-  
770 672.

771 Pogge von Strandmann P. A. E., Jones M. T., West A. J., Murphy M. J., Stokke E. W., Tarbuck  
772 G., Wilson D.J., Pearce C.R. and Schmidt D.N. (2021) Lithium isotope evidence for  
773 enhanced weathering and erosion during the Paleocene-Eocene Thermal Maximum. *Sci.*  
774 *Adv.* **7**, eabh4224.

775 Pogge von Strandmann P. A. E., Kasemann S. A. and Wimpenny J. B. (2020) Lithium and  
776 Lithium Isotopes in Earth's Surface Cycles. *Elements* **16**, 253-258.

777 Pogge von Strandmann P. A. E., Porcelli D., James R. H., van Calsteren P., Schaefer B.,  
778 Cartwright I., Reynolds B. C. and Burton K. W. (2014) Chemical weathering processes in  
779 the Great Artesian Basin: Evidence from lithium and silicon isotopes. *Earth Planet. Sci.*  
780 *Lett.* **406**, 24-36.

781 Pogge von Strandmann P. A. E., Schmidt D. N., Planavsky N. J., Wei, G., Todd, C. L. and  
782 Baumann K.-H. (2019) Assessing bulk carbonates as archives for seawater Li isotope  
783 ratios. *Chem. Geol.* **530**, 119338.

784 Roberts J., Kaczmarek K., Langer G., Skinner L. C., Bijma J., Bradbury H., Turchyn A. V.,  
785 Lamy F. and Misra S. (2018) Lithium isotopic composition of benthic foraminifera: A new  
786 proxy for paleo-pH reconstruction. *Geochim. Cosmochim. Acta* **236**, 336-350.

787 Rollion-Bard C., Vigier N., Meibom A., Blamart D., Reynaud S., Rodolfo-Metalpa R., Martin  
788 S. and Gattuso J.-P. (2009) Effect of environmental conditions and skeletal ultrastructure  
789 on the Li isotopic composition of scleractinian corals. *Earth Planet. Sci. Lett.* **286**, 63-70.

790 Shao L., Cui Y., Qiao P., Zhang D., Liu X. and Zhang C. (2017a) Sea-level changes and

791 carbonate platform evolution of the Xisha Islands (South China Sea) since the Early  
 792 Miocene. *Palaeogeogr. Palaeoclimatol. Palaeoecol.* **485**, 504-516.

793 Shao L., Li Q., Zhu W., Zhang D., Qiao P., Liu X., You L., Cui Y. and Dong X. (2017b) Neogene  
 794 carbonate platform development in the NW South China Sea: Litho-, bio- and chemo-  
 795 stratigraphic evidence. *Mar. Geol.* **385**, 233-243.

796 Stewart J. A., Gutjahr M., Pearce F., Swart P. K. and Foster G. L. (2015) Boron during meteoric  
 797 diagenesis and its potential implications for Marinoan snowball Earth  $\delta^{11}\text{B}$ -pH excursions.  
 798 *Geology* **43**, 627-630.

799 Swart P. K. (2015) The geochemistry of carbonate diagenesis: The past, present and future.  
 800 *Sedimentology* **62**, 1233-1304.

801 Taylor H. L., Duivesteyn I. J. K., Farkas J., Dietzel M. and Dosseto A. (2019) Technical note:  
 802 Lithium isotopes in dolostone as a palaeo-environmental proxy—an experimental approach.  
 803 *Clim. Past* **15**, 635-646.

804 Tissot F. L. H., Chen C., Go B. M., Naziemiec M., Healy G., Bekker A., Swart P. K. and  
 805 Dauphas N. (2018) Controls of eustasy and diagenesis on the  $^{238}\text{U}/^{235}\text{U}$  of carbonates and  
 806 evolution of the seawater ( $^{234}\text{U}/^{238}\text{U}$ ) during the last 1.4 Myr. *Geochim. Cosmochim. Acta*  
 807 **242**, 233-265.

808 Tomascak P. B., Magna, T., and Dohmen, R. (2016) Advances in Lithium Isotope Geochemistry  
 809 (pp. 1-195). Cham, Switzerland: Springer International Publishing.

810 Ullmann C. V., Campbell H. J., Frei, R., Hesselbo, S. P., Pogge von Strandmann P. A. E. and  
 811 Korte C. (2013) Partial diagenetic overprint of Late Jurassic belemnites from New Zealand:  
 812 Implications for the preservation potential of  $\delta^7\text{Li}$  values in calcite fossils. *Geochim.*



813 *Cosmochim. Acta* **120**, 80-96.

814 Vasconcelos C., McKenzie J. A., Warthmann R. and Bernasconi S. M. (2005) Calibration of  
 815 the  $\delta^{18}\text{O}$  paleothermometer for dolomite precipitated in microbial cultures and natural  
 816 environments. *Geology* **33**, 317-320.

817 Veizer J. (1983) Chemical diagenesis of carbonates: theory and application of trace element  
 818 technique. In *Stable Isotopes in Sedimentary Geology*, ed. M. A. Arthur, T. F. Anderson,  
 819 I. R. Kaplan, J. Veizer, L. S. Land, pp. III- I-100. Tulsa, Okla: Soc. Econ. Paleontol.  
 820 Mineral.

821 Vigier N., Gislason S.R., Burton K.W., Millot R. and Mokadem F. (2009) The relationship  
 822 between riverine lithium isotope composition and silicate weathering rates in Iceland.  
 823 *Earth Planet. Sci. Lett.* **287**, 434-441.

824 Vigier N., Rollion-Bard C., Levenson Y. and Erez J. (2015) Lithium isotopes in foraminifera  
 825 shells as a novel proxy for the ocean dissolved inorganic carbon (DIC). *C.R. Geosci.* **347**,  
 826 43-51.

827 Washington K. E., West A. J., Kalderon-Asael B., Katchinoff J. A. R., Stevenson E. I. and  
 828 Planavsky N. J. (2020) Lithium isotope composition of modern and fossilized Cenozoic  
 829 brachiopods. *Geology* **48**, 1058-1061.

830 Yi L., Jian Z., Liu X., Zhu Y., Zhang D., Wang Z. and Deng C. (2018) Astronomical tuning and  
 831 magnetostratigraphy of Neogene biogenic reefs in Xisha Islands, South China Sea. *Sci.*  
 832 *Bull.* **63**, 564-573.

833 Zachos J., Pagani M., Sloan L., Thomas E. and Billups K. (2001) Trends, rhythms, and  
 834 aberrations in global climate 65 Ma to present. *Science* **292**, 686-693.

835 Zhang F., Dellinger M., Hilton R. G., Yu J., Allen M. B., Densmore A. L., Sun H. and Jin Z. (2022)  
836 Hydrological control of river and seawater lithium isotopes. *Nat. Commun.* **13**, 3359.  
837 Zhao M., Planavsky N., Oehlert A. M., Wei G. and Gong Z. (2020) Simulating meteoric and mixing  
838 zone carbonate diagenesis with a two-dimensional reactive transport model. *Am. J. Sci.* **320**,  
839 599-636.

## Figure captions

**Fig. 1.** Bathymetric map of the South China Sea from Ocean Data View (<https://odv.awi.de>)

with locations of the studied XK-1 and Jiuzhang A and B drillcores and shallow-water coral skeletons, and stratigraphic columns, carbonate mineralogy (XRD analysis) and age models of the XK-1 and Jiuzhang A and B drillcores. The age model for XK-1 drillcore is modified from cyclostratigraphic and magnetostratigraphic data, together with foraminiferal biostratigraphy (Shao et al., 2017b; Yi et al., 2018).

**Fig. 2.** SEM (scanning electron microscopy) photomicrographs of the studied carbonate samples from the South China Sea. (A) Aragonite needles and nanograins of amorphous calcium carbonate on the surface of high-Mg calcite (Jiuzhang A core); (B) aragonite, high-Mg calcite and amorphous calcium carbonate (−15.7 m of the XK-1 drillcore); (C) aragonite needles on the surface of high-Mg calcite (−23.6 m of the XK-1 drillcore); (D) low-Mg calcites (meteoric diagenetic zone, −100.7 m of the XK-1 drillcore); (E) low-Mg calcites (marine diagenetic zone, −295.3 m of the XK-1 drillcore); (F) dolomites (marine dolomitization, −334.2 m of the XK-1 drillcore). The EDS (energy-dispersive spectrometry) is used to help distinguish the carbonate mineralogy.

**Fig. 3.** Profiles of carbonate mineralogy and  $\delta^{13}\text{C}$ ,  $\delta^{18}\text{O}$ ,  $\delta^7\text{Li}$  values along with Li and Sr contents for the XK-1, Jiuzhang A and B drillcores in the South China Sea. The orange symbols represent the primary or weakly diagenetic carbonates, mainly consisting of aragonite and high-Mg calcite; the wathet symbols represent the low-Mg calcites experiencing marine or meteoric diagenesis; and the tan symbols represent the dolomites. The vertical gray bars correspond to  $\delta^7\text{Li}$  values of modern seawater, and inorganic aragonite and

862 calcite precipitating from modern seawater (Marriot et al., 2004b; Gabitov et al., 2011;  
863 Heathorne and James, 2006; Misra and Froelich, 2012; Pogge von Strandmann et al., 2019).

864 **Fig. 4.** The results of  $\delta^{13}\text{C}$ ,  $\delta^{18}\text{O}$ ,  $\delta^7\text{Li}$  and Li contents of different coral species from the  
865 Nansha Islands and Hainan Island, South China Sea. The shaded areas represent  $\delta^7\text{Li}$  ranges  
866 of modern seawater, inorganic aragonite and calcite precipitating from modern seawater  
867 (Marriot et al., 2004b; Gabitov et al., 2011; Heathorne and James, 2006; Misra and Froelich,  
868 2012; Pogge von Strandmann et al., 2019), and Jiuzhang A and B cores.

869 **Fig. 5.** Cross-plots of  $\text{Li}/(\text{Ca}+\text{Mg})$  vs.  $\text{Mg}/(\text{Ca}+\text{Mg})$  and  $\text{Sr}/(\text{Ca}+\text{Mg})$  ratios for the XK-1,  
870 Jiuzhang A and B drillcores in the South China Sea. The red stars represent the typical  
871 compositions of aragonite, high-Mg calcite, low-Mg calcite and dolomite (Dellinger et al.,  
872 2018, 2020; Pogge von Strandmann et al., 2019). The gray dashed lines represent the mixing  
873 of different carbonate minerals.

874 **Fig. 6.** Relationships between  $\delta^7\text{Li}$  values and  $\text{Li}/(\text{Ca}+\text{Mg})$ ,  $\text{Mg}/\text{Ca}$ ,  $\delta^{13}\text{C}$ ,  $\delta^{18}\text{O}$  values for XK-  
875 1, Jiuzhang A and B drillcores in the South China Sea, as well as their comparisons with the  
876 Bahamian aragonite and Atlantic core-top calcite samples from Pogge von Strandmann et al.  
877 (2019).

878 **Fig. 7.** Temporal changes in  $\delta^{13}\text{C}$ ,  $\delta^{18}\text{O}$  and  $\delta^7\text{Li}$  records of XK-1 drillcore from the middle  
879 Miocene to the present time and their comparisons with planktonic foraminiferal records. The  
880 foraminifera  $\delta^7\text{Li}$  curve is modified from Misra and Froelich (2012). The planktonic  
881 foraminiferal  $\delta^{13}\text{C}$  and  $\delta^{18}\text{O}$  records of northern South China Sea are modified from ODP  
882 Sites 1147 and 1148 (Cheng et al., 2004). The age model of the XK-1 drillcore, South China

Sea is modified by astronomical tuning from Yi et al., (2018), assuming relatively constant depositional rates in the XK-1 drillcore.

**Fig. 8.** Comparisons of shallow-water carbonate  $\delta^7\text{Li}$  records during the marine diagenesis (dolomitization) and meteoric diagenesis from the South China Sea (this study) and the Bahamas (Dellinger et al., 2020).

**Fig. 9.** Histograms of  $\delta^7\text{Li}$  in primary inorganic carbonates and post-depositional (marine or meteoric diagenetic) carbonate sediments from the latest Miocene, during which seawater Li isotope compositions are considered to be constant and close to modern seawater values (data compiled from Pogge von Strandmann et al., 2019; Dellinger et al., 2020 and this study).

**Fig. 10.** Modeling results for  $\delta^7\text{Li}$  changes in shallow-water carbonates via interaction with (A) seawater and (B) freshwater, and cross-plots of (C)  $\delta^7\text{Li}$  and  $\text{Li}/(\text{Ca}+\text{Mg})$ , (D)  $\delta^7\text{Li}$  and  $\text{Mg}/\text{Ca}$ , (E)  $\delta^7\text{Li}$  and  $\delta^{13}\text{C}$ , (F)  $\delta^7\text{Li}$  and  $\delta^{18}\text{O}$  during the marine dolomitization, neomorphism from aragonite/high-Mg calcite to low-Mg calcite, and meteoric diagenesis (modified from Ahm et al., 2018, see Supplementary information for parameter description). The  $\delta^7\text{Li}$  values of the bulk carbonates evolve at the specific reaction rate when fluids flow through the sediment pile at a constant advection rate. The  $\delta^7\text{Li}$  trajectory (y-axis) is determined by increasing the cumulative mass of fluid relative to sediment over time (x-axis). In the model, boxes denote the thickness of the sediment column with  $1\text{ m}^3$  of volume for each box. The box 1 represents the uppermost part, and box N represents the deepest part of the sediment pile, which are denoted as black arrows in (C), (D), (E), (F). The gray lines in (C), (D), (E), (F) represent percentiles of the degree of alteration of bulk sediments (from 0% to 100%). The

904 fully diagenetic sediments are represented by the diagenetic end-member using thick blue  
905 lines in (C), (D), (E), (F).

**Table 1. Parameters used in the early marine diagenetic model**

Items	Definition	Value	Notes or References
$P$	porosity	0.4	
$\rho_f$	fluid density	1.0125 g/mL	
$\rho_s$	solid density	1.8 g/mL	
$R$	reaction rate	10% myr <sup>-1</sup>	Ahm et al., 2018
$u$	advection rate	10 cm·yr <sup>-1</sup>	Ahm et al., 2018
$n$	box number	50	Ahm et al., 2018
$m$	stoichiometric scaling factor	element/Ca	
$M_f$	concentrations of element in initial fluid	Li <sub>seawater</sub> = 265 nM; Li <sub>freshwater</sub> = 2.16 nM Ca <sub>seawater</sub> = 10.6 mM; Ca <sub>freshwater</sub> = 2.1 mM C <sub>seawater</sub> = 2.3 mM; C <sub>freshwater</sub> = 2.3 mM	Misra and Froelich, 2012, Huh et al., 1998; Chester and Jickells, 2012
$M_s$	concentrations of element in primary sediment	Ca = 39% Mg = 2500 ppm C = 12%	Primary carbonate minerals
$\delta_f$	isotopic value of initial fluid	$\delta^7\text{Li}_{\text{seawater}} = 31\text{‰}$ ; $\delta^7\text{Li}_{\text{freshwater}} = 20\text{‰}$ $\delta^{13}\text{C}_{\text{seawater}} = 3\text{‰}$ ; $\delta^{13}\text{C}_{\text{freshwater}} = -4\text{‰}$ $\delta^{18}\text{O}_{\text{seawater}} = -29\text{‰}$ ; $\delta^{18}\text{O}_{\text{freshwater}} = -39\text{‰}$	Misra and Froelich, 2012, Mayfield et al., 2021; Cheng et al., 2004; this study
$\delta_s$	isotopic value of primary sediments	$\delta^7\text{Li}_{\text{aragonite}} = 21\text{‰}$ ; $\delta^7\text{Li}_{\text{HMC}} = 25\text{‰}$ $\delta^{13}\text{C} = 1.5\text{‰}$ $\delta^{18}\text{O} = -3.5\text{‰}$ ;	Dellinger et al., 2018, Pogge von Strandmann et al., 2019; Murphy et al., 2022; this study;
$\alpha$	isotope fractionation factors during the recrystallization	Estimated $\alpha_{\text{Li}} = 0.999$ ; $\alpha_{\text{C}} = 0.9988$ ; $\alpha_{\text{O}} = 1.03106$ (calcite), 1.02845 (dolomite)	Dellinger et al., 2020, Murphy et al., 2022; this study; Emrich et al., 1970; O'Neil et al., 1969, Vasconcelos et al., 2005
$K_d^{\text{Li}}$	partition coefficients for diagenetic low-Mg calcite and dolomite	$K_d^{\text{Li}} = 0.001$ (low-Mg calcite), 0.002 (dolomite)	Low-Mg calcite: Marriott et al., 2004a,b; Füger et al., 2019 Dolomite: estimated in this study, considering measured Li contents in low-Mg calcite and dolomite from the XK-1 drillcore

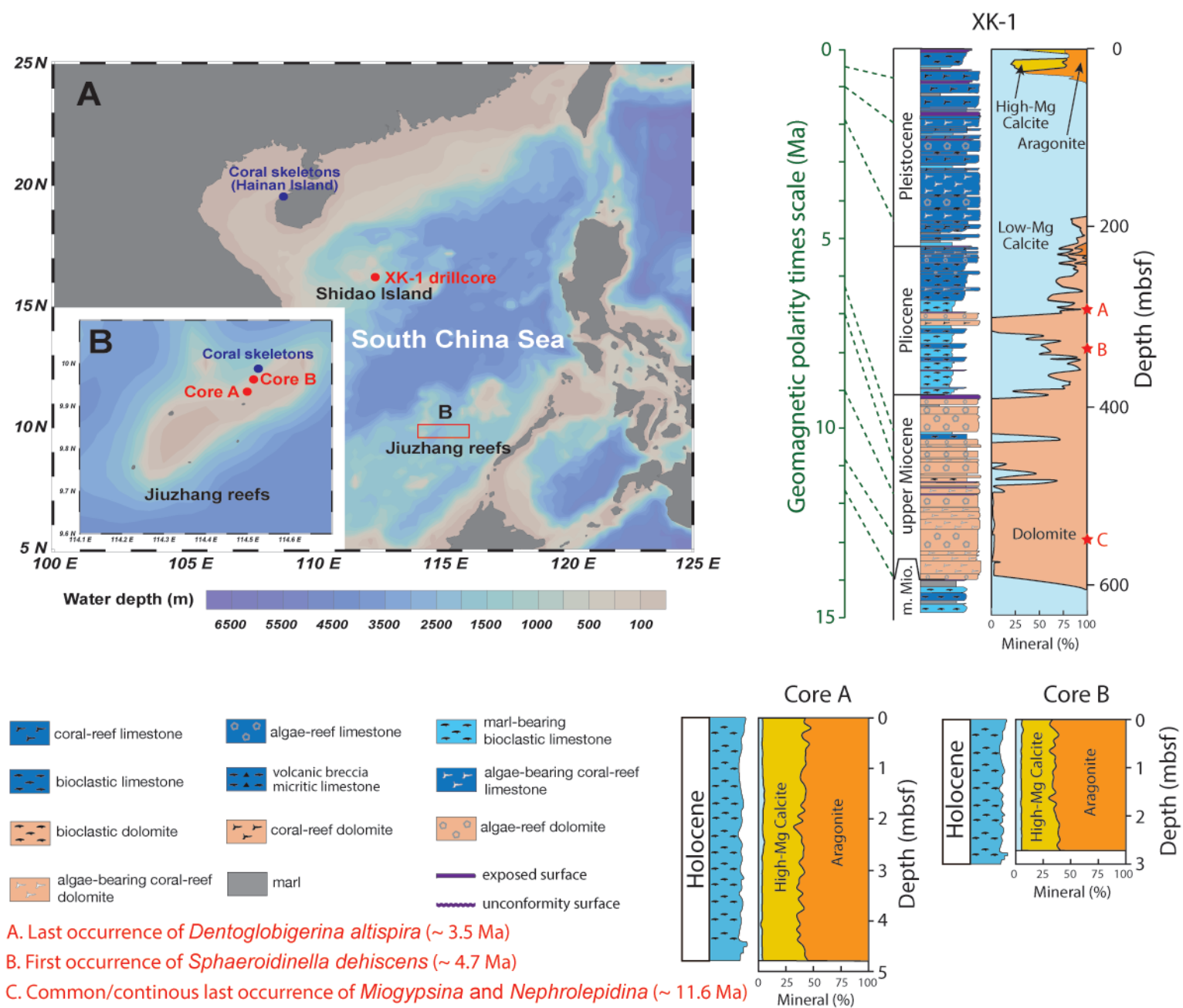




Figure 2

[Click here to access/download;Figure;Fig. 2\\_GCA\\_R2.pdf](#)

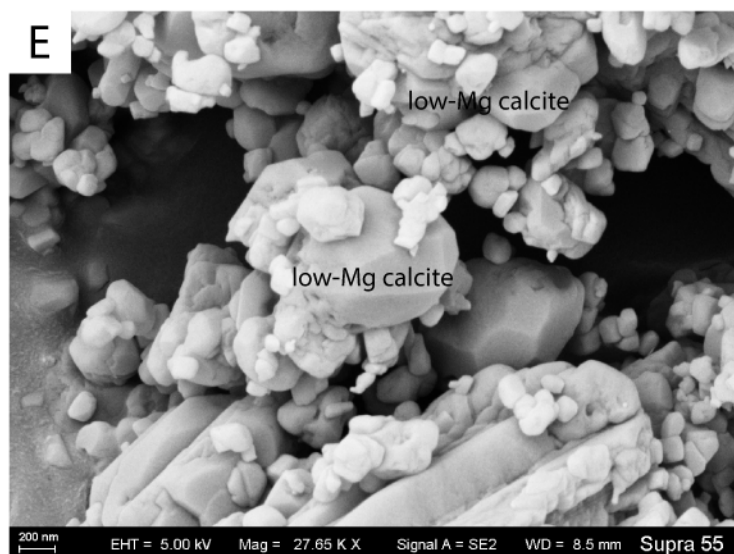
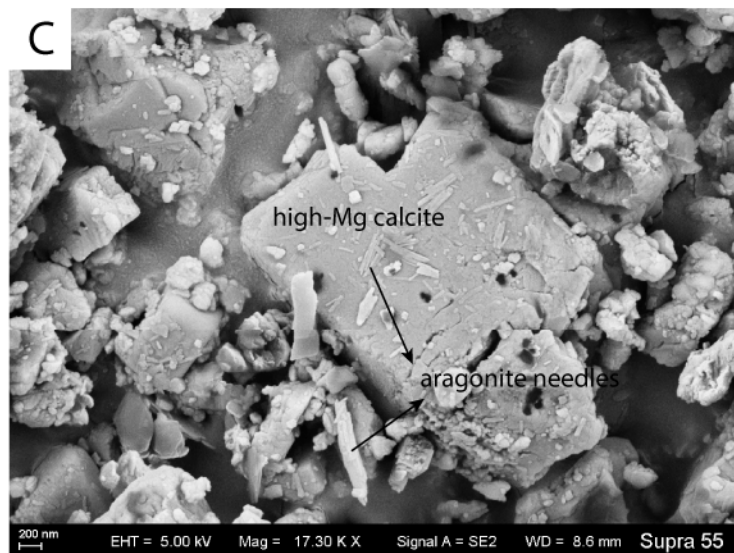
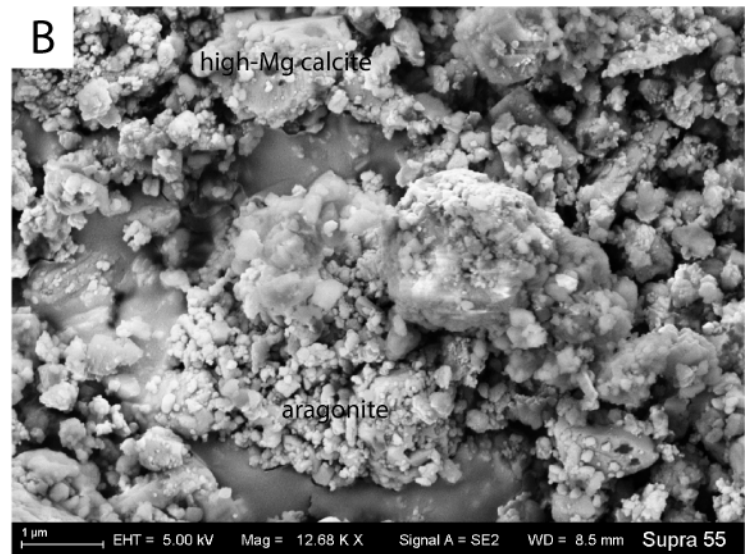
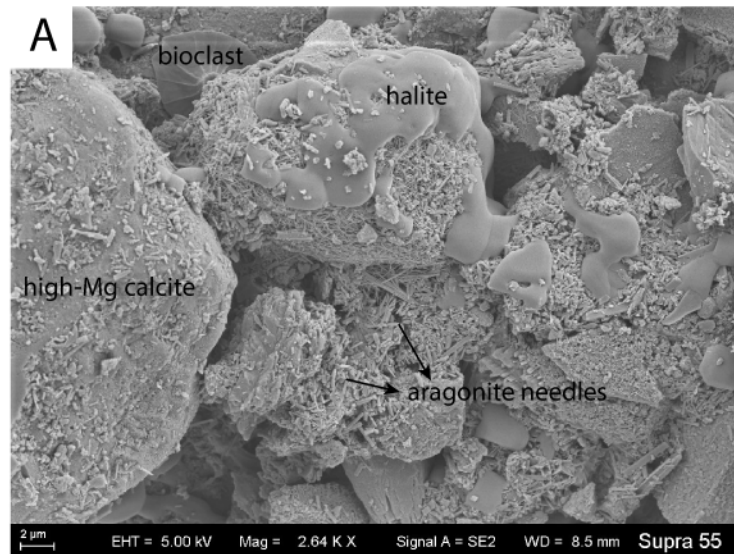
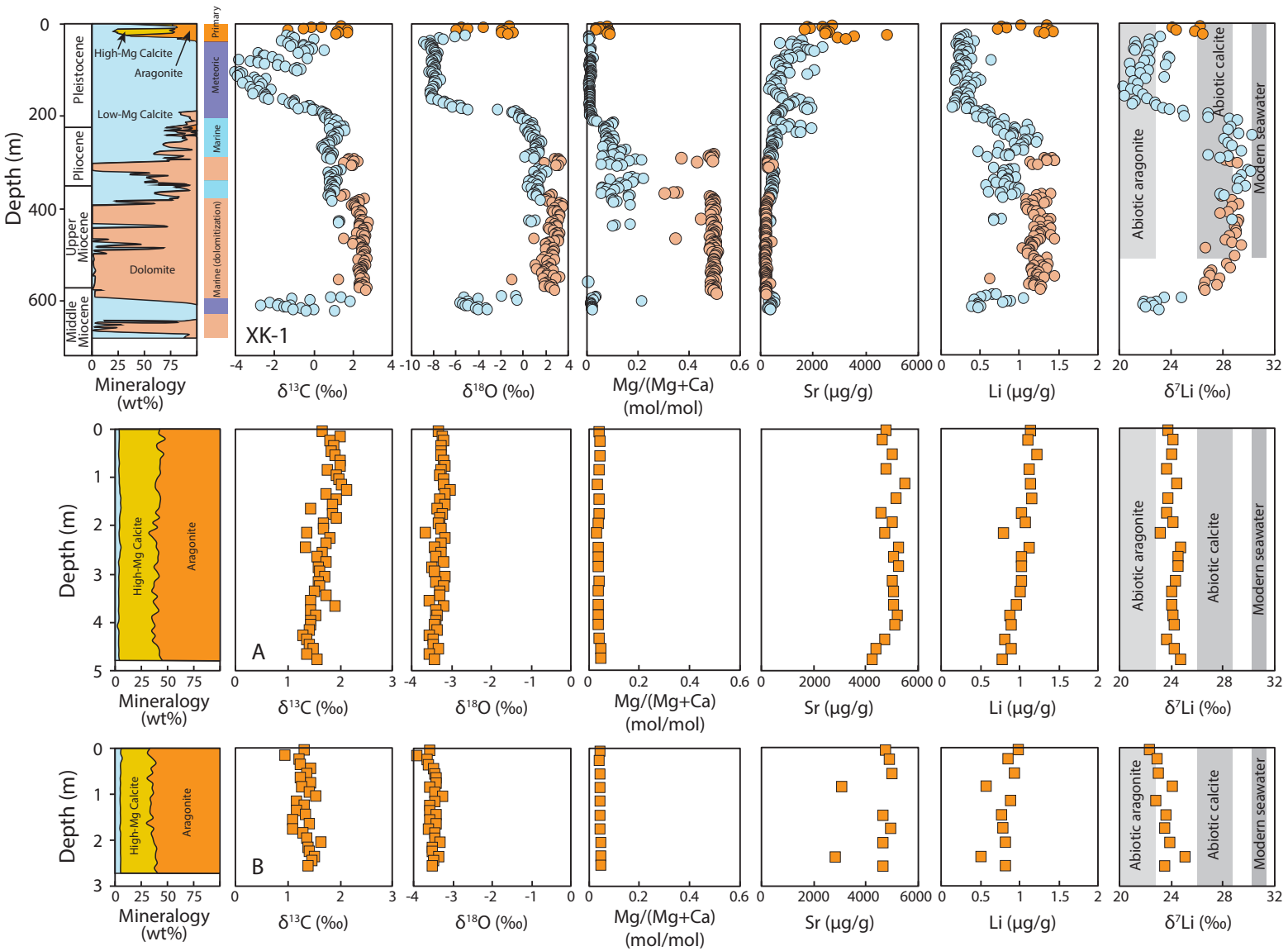
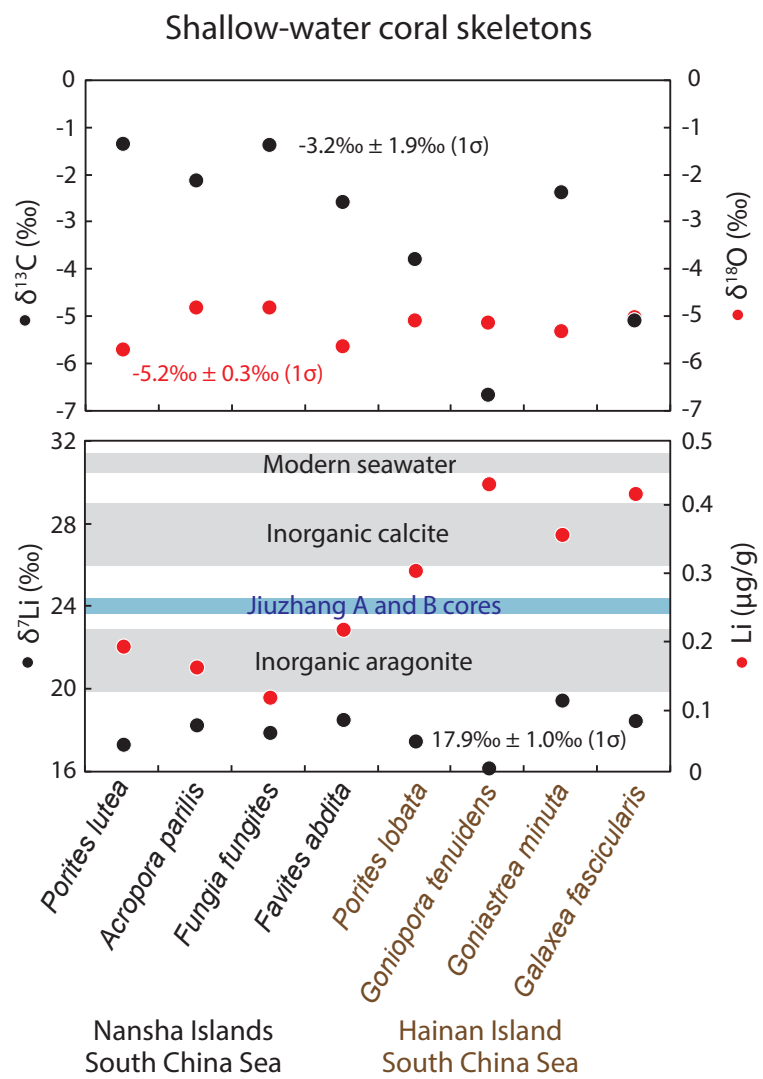
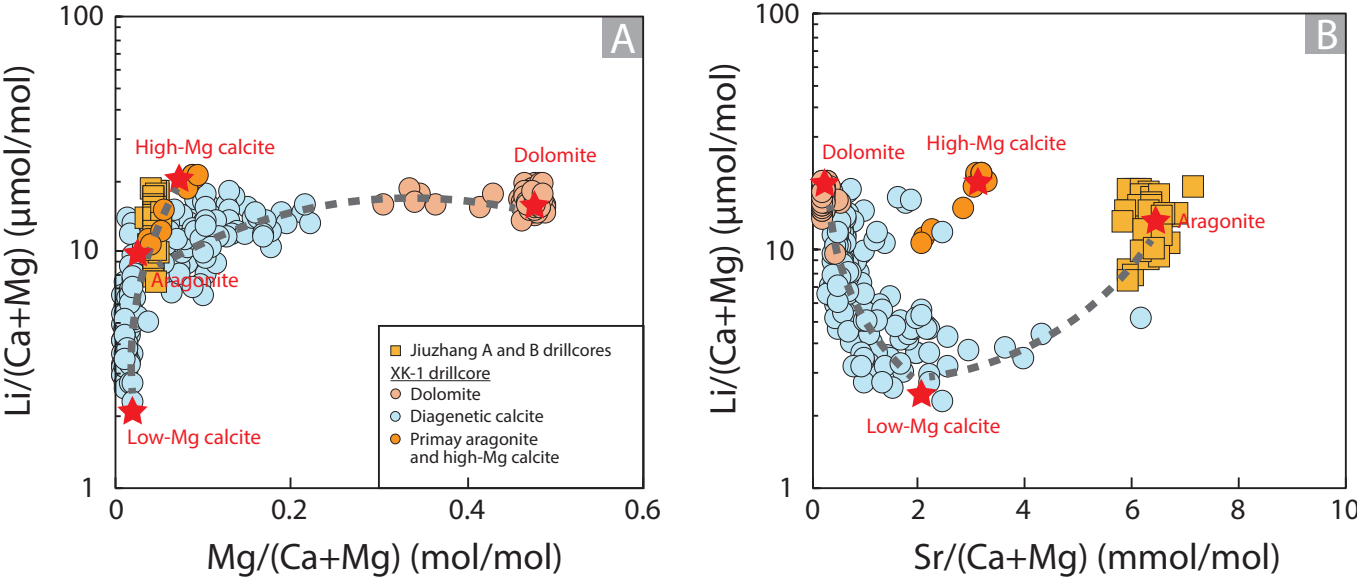


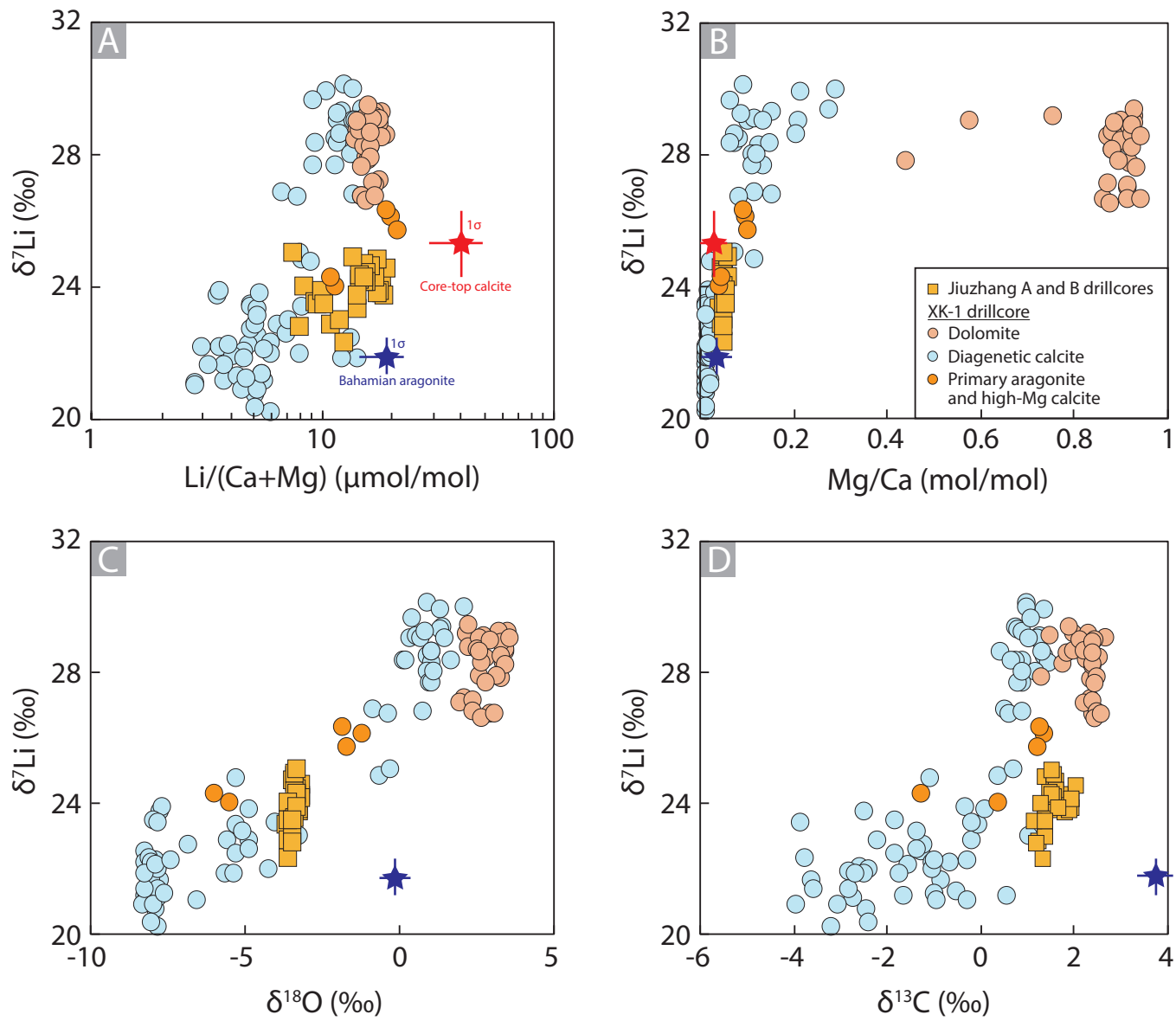
Figure 3

[Click here to access/download;Figure;Fig. 3\\_GCA\\_R2.pdf](#)











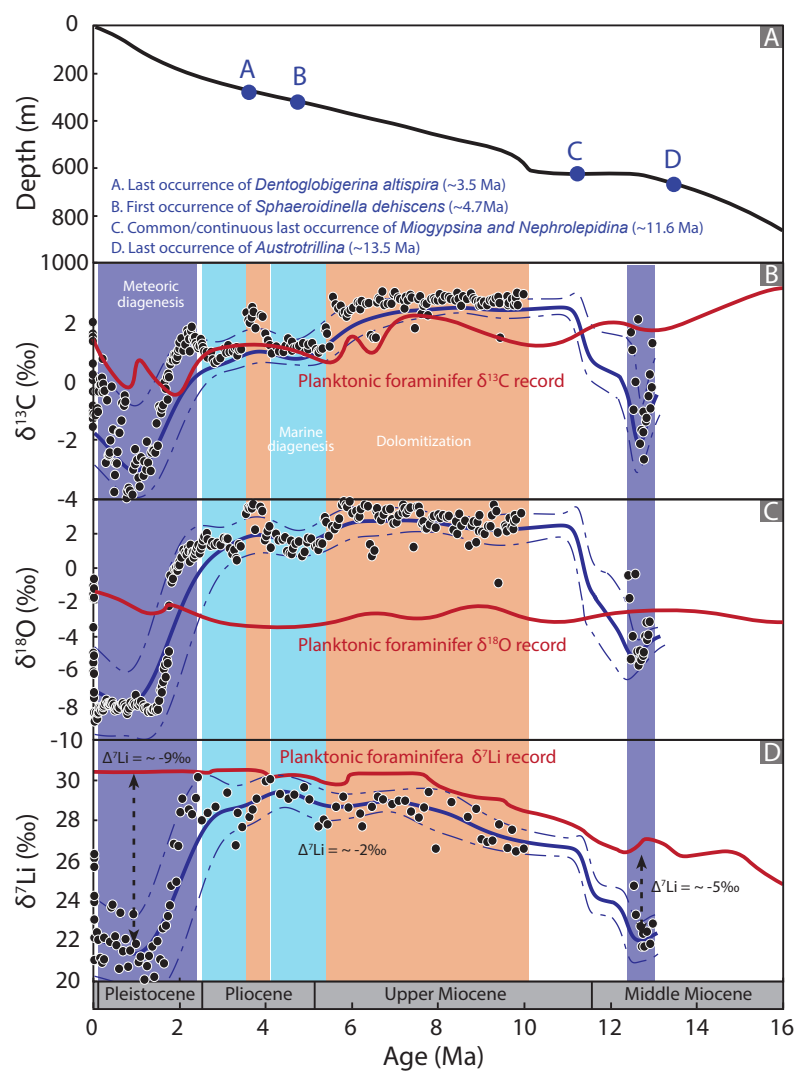
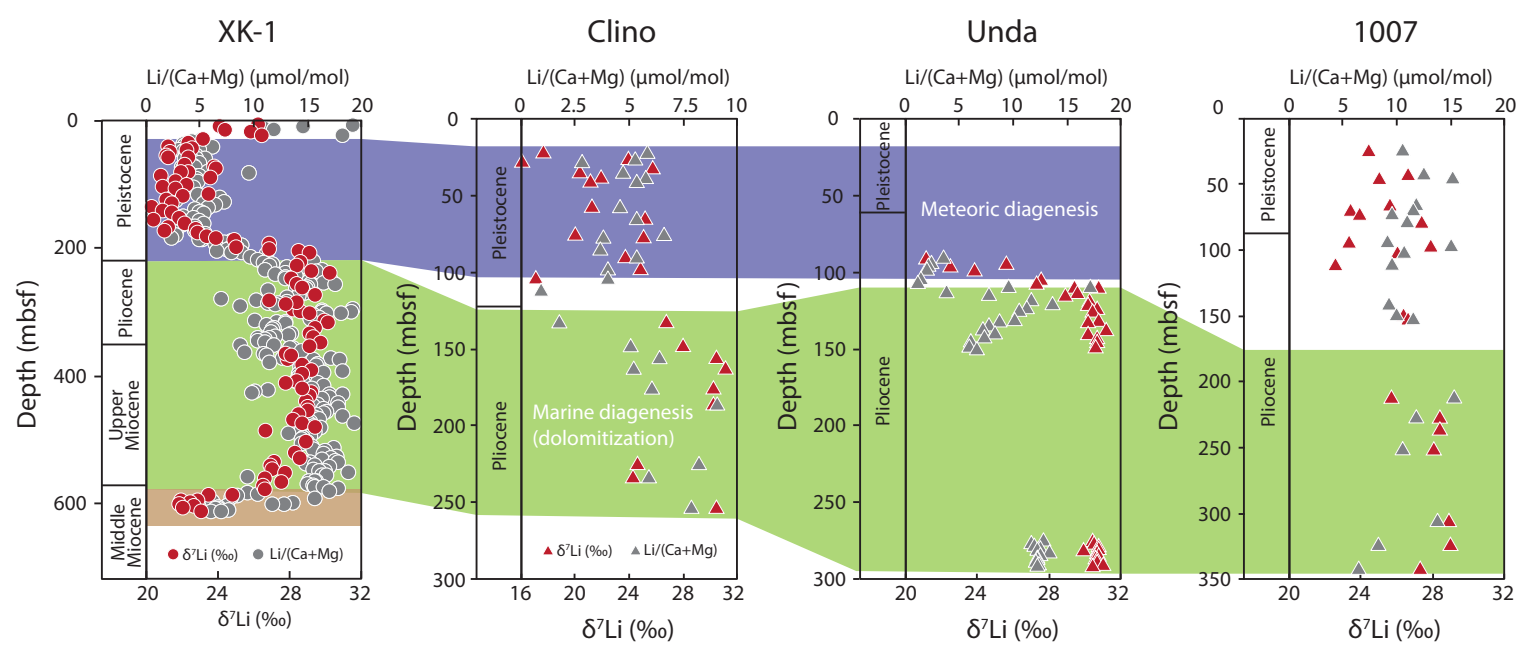


Figure 8

[Click here to access/download;Figure;Fig. 8\\_GCA\\_R2.pdf](#)



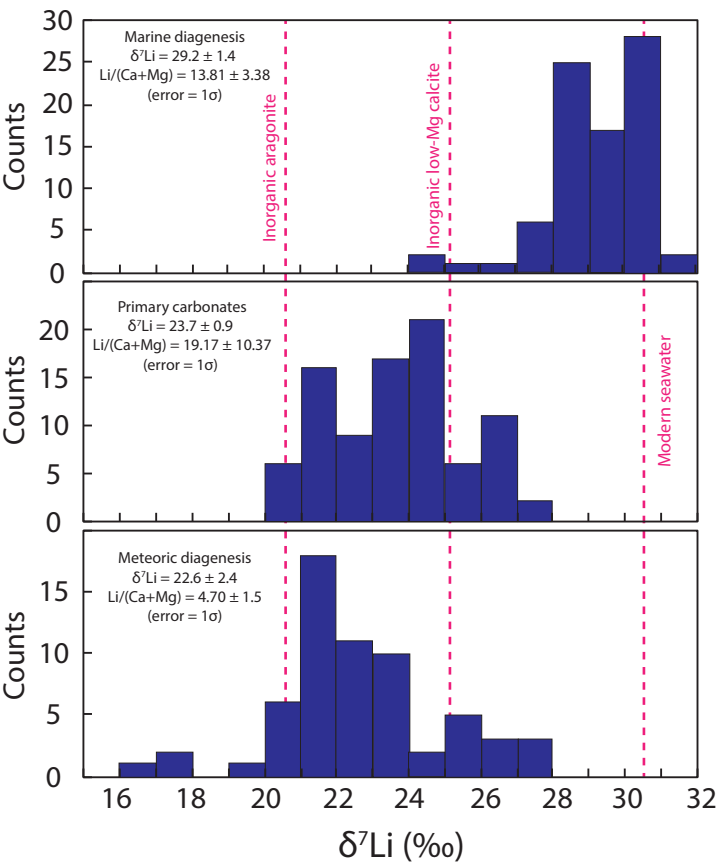




Figure 10

[Click here to access/download;Figure;Fig. 10\\_GCA\\_R2.pdf](#)